Contributions to Mineralogy and Petrology (2019) 174:56
https://doi.org/10.1007/s00410-019-1591-5

ORIGINAL PAPER

Formation of rapakivi feldspar in the Deer Isle Granite Complex, coastal Maine: in situ lead isotope and trace-element analysis

William Desmond O'Brien[1] · Michael J. Dorais[1] · Eric H. Christiansen[1] · David Gibson[2]

Received: 7 December 2018 / Accepted: 15 May 2019 / Published online: 1 June 2019

Abstract

Rapakivi and alkali feldspar phenocrysts from the Devonian Deer Isle Granite Complex, Maine were investigated to see if magma mixing or isothermal decompression was responsible for their formation. Pb-isotope and trace-element analyses of alkali feldspar ovoids and their plagioclase inclusions were obtained by LA-ICP-MS to determine the characteristics of the initial magma; these were compared with the plagioclase mantles. Rapakivi grains show a decrease in Pb-isotopic values and an increase in Ba, La, and Ce concentrations from the ovoids and inclusions to the innermost plagioclase mantles adjacent to the ovoids. These variations, along with CL imagery of quartz phenocrysts, indicate an open system with compositional changes in the magma chamber occurring during rapakivi feldspar growth. Repeated episodes of magma mixing/replenishment by Ba and LREE enriched magmas with lower Pb-isotopic ratios (along with hybridized variations with the host magma) created localized dissolution of alkali feldspar and quartz. Alkali feldspar phenocrysts proximal to these zones of thermal perturbation were first resorbed and then mantled by plagioclase that records the more primitive signature of the more mafic melt. Pb-isotopic values and Ba, La, and Ce concentrations trend back to the initial magma composition at the mantle rims as the effects of the mixing event dissipated. For grains that were somewhat more distal to these zones of mixing, resorption of the alkali feldspar crystals did not occur, yet the fresh supply of Ba resulted in Ba-rich alkali feldspar mantles over Ba-poor alkali feldspar cores. Other alkali feldspar crystals were too far from the site of mixing; hence, they lack any evidence of open system crystallization. As crystallization of the chamber continued along solidification fronts, batches of cooler crystal-rich magmas settled *en masse* to the floor. Disaggregation of these batches during settling, and subsequent accumulation on the reservoir floor, brought grains with disparate crystallization histories together. Filter pressing of the cumulate pile flushed highly evolved melts/fluids out from interstitial pores to the high silica, upper portions of the chamber. The crystallization, transportation, and juxtaposition of disparate types of feldspar phenocrysts suggest that a relatively large and active magma chamber, periodically recharged by localized batches of melt, must have existed. In this case, it is clear that rapakivi mantled feldspars are the result of magma mixing; such interpretations may apply to many other occurrences as well.

Keywords Deer Isle Granite · Rapakivi feldspar · Magma mixing

Introduction

The rapakivi texture (sensu stricto) of granites, first identified by Sederholm (1891), and later further defined by Vorma (1976), is characterized by: (1) ovoidal alkali feldspar phenocrysts, the majority of which are partially to completely mantled by plagioclase shells, and (2) the ubiquitous presence of two generations of alkali feldspar and quartz, with the first generation of quartz crystallizing as high (β) quartz and idiomorphic in nature. Granites exhibiting this texture are called rapakivi granites (Vorma 1976). Vorma limited the term rapakivi granite (sensu stricto) to describe only Precambrian granites (ca.

Communicated by Timothy L. Grove.

Electronic supplementary material The online version of this article (https://doi.org/10.1007/s00410-019-1591-5) contains supplementary material, which is available to authorized users.

✉ Michael J. Dorais
dorais@byu.edu

[1] Department of Geological Sciences, Brigham Young University, Provo, UT, USA

[2] Department of Geology, University of Maine Farmington, Farmington, ME 04938, USA

1700 Ma) found largely in the Baltic Shield, whereas Haapala and Rämö (1992) modified the definition of rapakivi granites to be genetically A-type and not limited to being Precambrian in age. In this paper, the term rapakivi feldspars (sensu lato) will be used to describe plagioclase-mantled alkali feldspars regardless of their age, relation to orogenesis, or tectonic setting.

The process by which rapakivi feldspars formed has been hypothesized by many authors (e.g., Sederholm 1891; Whitney 1975; Stull 1979; Hibbard 1981; Bussy 1990; Nekvasil 1991; Stimac and Wark 1992; Dempster et al. 1994; Eklund and Shebanov 1999) and summarized by Rämö and Haapala (1995). Of these, three are more widely accepted and are described below.

Nekvasil (1991), building on Whitney's work (1975), hypothesized that rapakivi growth could occur if an ascending granitic magma (1) did not become saturated with respect to H_2O, (2) cooling rates are within ~ 5–10 °C/kbar, (3) both alkali feldspar and plagioclase were present in the magma prior to ascent, and (4) initial temperatures of the magma were low enough to prevent complete resorption of alkali feldspar. With these conditions met, alkali feldspar would destabilize, while plagioclase remained stable during decompression (Eklund and Shebanov 1999). The resorbed ovoidal alkali feldspars would then provide nuclei for continued growth of plagioclase.

The second hypothesis holds that the formation of rapakivi feldspars occurs through magma mixing (Hibbard 1981; Wark and Stimac 1992; Stimac and Wark 1992). Here, two contrasting magmas (mafic and granitic) mix and, either completely or partially, hybridize. A granitic magma mixing with a hotter, more mafic magma will experience resorption of alkali feldspar and quartz due to increases in the system's temperature. Continued stability of plagioclase allows plagioclase to nucleate on the resorbed alkali feldspars (Hibbard 1981), and is followed by the additional growth of quartz over the resorbed quartz and renewed alkali feldspar crystallization when lower temperatures are again reached.

A third hypothesis has also been presented by Dempster et al. (1994). They propose that the rapakivi texture is formed by the subsolidus exsolution of plagioclase in the alkali feldspars. Here, plagioclase migrates towards the rims and thus "mantles" the alkali feldspars. Similarly, Mondal et al. (2017) suggest that rapakivi forms via subsolidus deuteric alteration of feldspar by a subsolidus dissolution–reprecipitation process. To date, the subsolidus hypotheses have not been widely explored (cf. Rämö and Haapala 2005) and most studies support the first or second hypothesis (Eklund and Shebanov 1999; Narayana et al. 2000; Wang et al. 2008; Müller et al. 2008; Heinonen et al. 2010, Vernon 2016). However, no consensus has been reached as to which is responsible for the formation of rapakivi textures. This may be due to the fact that not just one process is involved in the development of the distinctive rapakivi texture; or there is a lack of means to determine what the process was.

We have attempted to resolve the rapakivi problem for the feldspars of the Deer Isle Granite Complex of coastal Maine. This study includes: (1) trace-element analyses by laser ablation inductively coupled plasma mass spectrometry (LA-ICP-MS) of plagioclase inclusions within alkali feldspar ovoids, plagioclase mantles, and phenocrystic plagioclase within the granite matrix; (2) in situ laser ablation multicollector inductively coupled plasma mass spectrometry (LA-MC-ICP-MS) Pb-isotopic analyses of alkali feldspar ovoids and plagioclase inclusions within, plagioclase mantles and plagioclase phenocrysts; and (3) acquisition of cathodoluminescence images of zoning in quartz and rapakivi phenocrysts. We use these data to show that magma mixing is the best explanation for the production of mantled feldspars in the Deer Isle Granite Complex.

Geological background

The Deer Isle Granite Complex is located in East Penobscot Bay, 65 km south of Bangor, Maine. The complex is part of the Coastal Maine magmatic province of eastern coastal Maine (Hogan and Sinha 1989). The province contains over 100 post-tectonic, late Silurian-to-Mississippian plutons (Hogan and Mataragio 2006) that intruded a collage of northeast-trending, fault-bounded, lithotectonic terranes of Proterozoic-to-Devonian rocks (Hogan and Sinha 1989). Magmatism within the Coastal Maine Magmatic Province is thought to have occurred in an extensional environment within a transtensional regime of a transcurrent fault system (Hogan and Sinha 1989).

The Deer Isle Granite Complex (Fig. 1) was first subdivided into two facies by Stewart (1956): the Stonington and Oak Point granites. Hooks (2003) divided the complex further: the Flye Point and Oak Point facies of the Oak Point granite, and the Settlement Quarry and Crotch Island facies of the Stonington granite. Lux et al. (2007) interpreted the complex to represent a magma chamber that has been tilted, allowing for a cross-sectional view, with the Flye Point facies representing the bottom of the chamber and the Crotch Island facies representing the top (Fig. 1).

Due to the lack of internal contacts, the major feature distinguishing each facies is the proportion of rapakivi feldspar grains (sensu lato), called plagioclase-mantled K-feldspar by Lux et al. (2007). The Flye Point facies has the most abundant rapakivi feldspars at 614 per m^2, and represents the northeastern, base of the pluton. To the southwest, and towards the top of the intrusion, the Oak Point facies, has an average of 357 rapakivi feldspars per m^2. The Settlement Quarry and Crotch Island, also representing the upper portions of the chamber, have the least rapakivi feldspar: 95 and

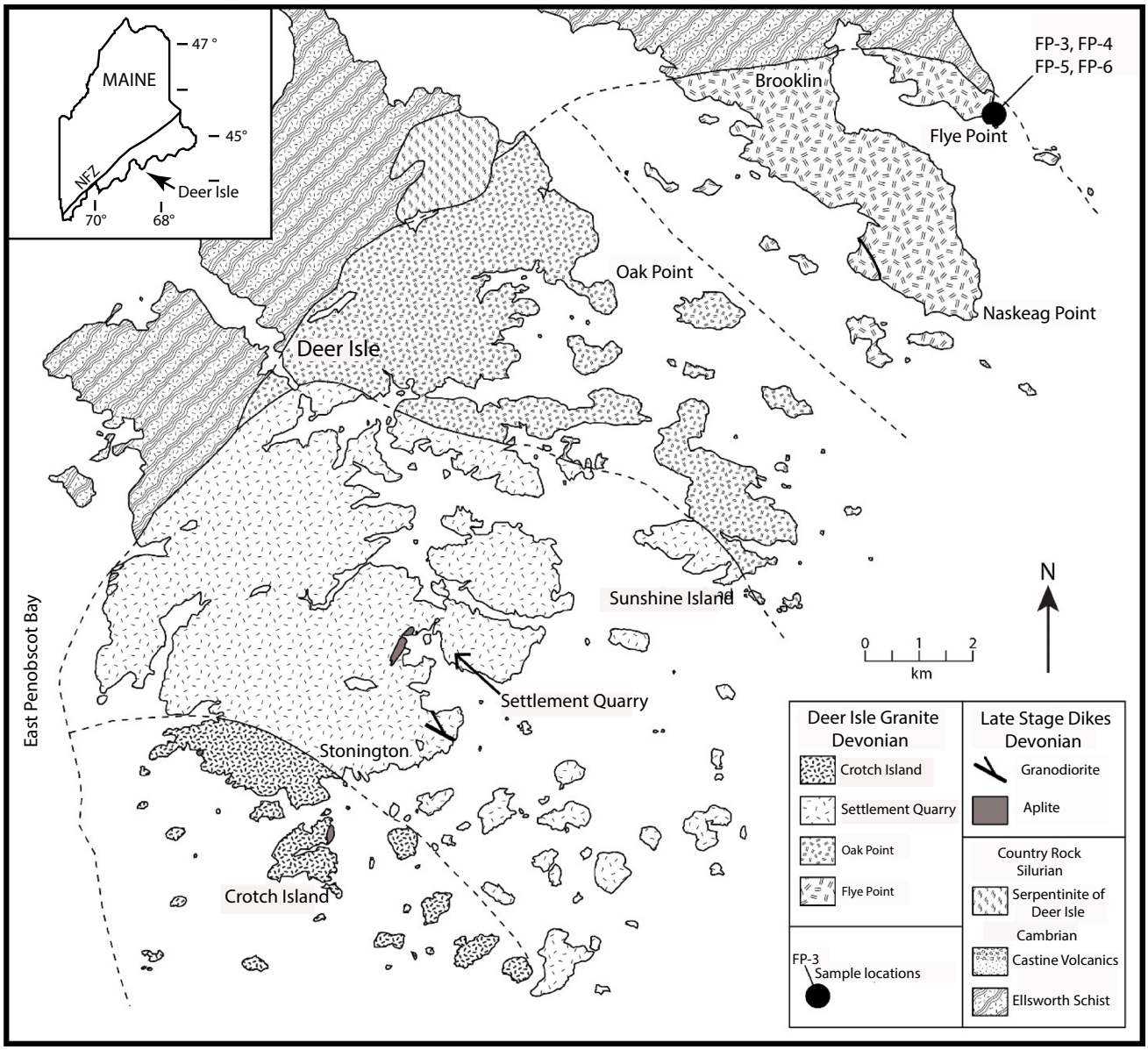

Fig. 1 Geological map of the Deer Isle Granite Complex (after Lux et al. 2007)

71 per m^2, respectively (Lux et al. 2007). We focused our study on the basal Flye Point facies because of its abundance of large, rapakivi feldspar crystals (Fig. 2a).

Mafic, intermediate, and felsic enclaves are present throughout the pluton, with abundances decreasing upward (mimicking the pattern found for the rapakivi feldspar concentrations). They are angular to disc-shaped to almost spherical and range from 1 cm to several meters in size (Fig. 2b). Alignment of these enclaves generally parallel feldspar foliations found throughout the Flye Point and Oak Point facies (Johnston 2001). Porphyritic enclaves often contain rounded (resorbed) plagioclase, alkali feldspars, rapakivi feldspars, and quartz ocelli (Lux et al. 2007). Fine-grained quartz diorite and diorite enclaves are generally smaller (< 20 cm) and rounded compared to the more felsic ones. Accessory minerals within the intermediate enclaves include apatite, titanite (matrix and ocelli), zircon, and allanite (Hooks 2003; Lux et al. 2007).

Methods

Rapakivi and alkali feldspars analyzed were collected from the type locality for the Flye Point facies (Flye Point, Deer Isle, Maine; Fig. 1). Electron microprobe analyses and X-ray dot maps for feldspars were completed at Brigham Young

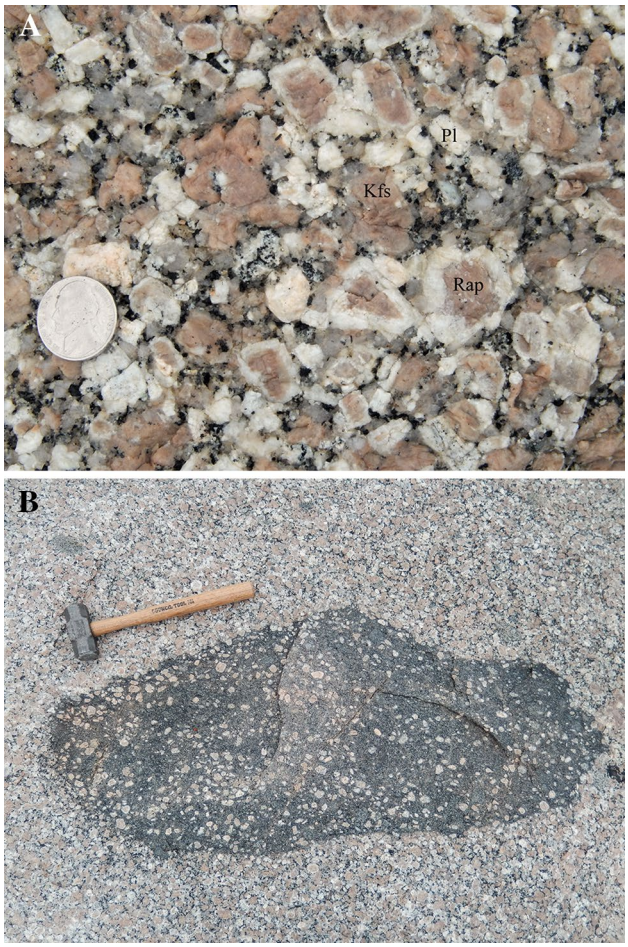

Fig. 2 **a** Granitic rocks of the Flye Point facies. Rapakivi feldspars (Rap) show variable degrees of rounding of the cores, some are rounded, and others are more rectangular. Other alkali feldspar crystals (Afs) are not mantled at all. Plagioclase (Pl) occurs both as individual phenocrysts and as mantles on alkali feldspar ovoids. **b** Mafic enclave at Flye Point has been interpreted as evidence for magma mixing (Lux et al. 2007). The enclave contains abundant alkali feldspar phenocrysts incorporated from the granitic host magma

University using a Cameca SX50 electron microprobe. Analyses used a 15 kV accelerating voltage, 10 nA beam current with a 10 µm beam diameter. Representative analyses are given in Supplementary Table 1.

Wavelength-dispersive X-ray spectroscopy element maps of feldspars were constructed for Si Kα, Ca Kα, K Kα, and Ba Lα and are presented in Figs. 3, 4, 5, 6, 7, and 8. Element maps were obtained using a 15 kV accelerating voltage, a 40 nA beam current (Ba Lα used 100 nA), a 10 µm beam diameter.

In situ trace-element LA-ICP-MS analyses of plagioclase were carried out at the W.M. Keck Collaboratory for Plasma Mass Spectrometry at Oregon State University using a Photon Machines Analyte G2 193 nm excimer laser coupled to a Thermo X-Series II quadrupole ICP-MS and followed analytical techniques outlined by Kent et al. (2004). Spot analyses had a diameter of 50 µm, a pulse frequency of 7 Hz, and an ablation time of 30–45 s. Background measurements were taken for 30 s prior to start of each run with a 30 s signal washout period between each ablation. Trace elements analyzed, and dwell times for each element are presented in Supplementary Table 2.

U.S. Geological Survey glass standards GSE-1G, BHVO-2G, BCR-2G, and National Institute of Standards NIST-612 and NIST-613 were used during each run of analyses, with GSE-1G used to standardize between every 8–10 unknowns to monitor accuracy and precision of analytical run. Analysis uncertainties are generally below 5% standard error (SE) for most elements with the following exceptions: ^{25}Mg, ^{85}Rb, ^{89}Y ^{147}Sm, and ^{157}Gd > 10%, ^{146}Nd > 15%, and ^{90}Zr, ^{93}Nb, ^{159}Tb, and ^{172}Yb generally below detection limits. Raw data were processed using the in-house LaserTram and LaserCalc software (Kent et al. 2004) using ^{43}Ca as the internal standard. Electron microprobe analyses for CaO concentrations of each sample spot were used to reduce the data.

In situ Pb-isotope compositions of plagioclase and alkali feldspar were analyzed by MC-ICP-MS, using a Photon Machines Analyte G2 193 nm excimer laser coupled to an Nu Plasma Multi Collector ICP Mass Spectrometer at the W.M. Keck Collaboratory for Plasma Mass Spectrometry at Oregon State University (Supplementary Table 3). Analytical techniques followed those used by Kent (2008) and glasses NIST-612 and BCR-2G were used as standards. Each analysis consisted of a 135 µm spot diameter, a pulse frequency of 10 Hz, and a shot count of 225. Pb-isotope measurements obtained consisted of ^{206}Pb, ^{207}Pb, and ^{208}Pb; the minor ^{204}Pb isotope was also measured, but results are not presented here due to difficulty in its detection above background in these samples. Because of variable alteration of the feldspars, continuous linear traverses from core to rim were not obtained by LA-ICP-MS analyses for most grains, and only the fresh portions of the feldspars were analyzed. Where this was the case, analyses are ordered on the graphs according to their relative positions from core to rim (Figs. 11, 13, 14).

Cathodoluminescence (CL) imagery was conducted at Brigham Young University using an FEI/Philips XL30 FEG environmental scanning electron microscope with a GATAN MiniCL detector. An accelerating voltage of 15 kV and a spot size of 6 µm were used for each image with the stage tilted 12°–15° from horizontal. Scanning rates were at 116 ms/line scan resulting in images roughly 1700 × 2300 µm. Because grains were much larger than maximum image size (e.g., > 2 cm^2), multiple images were taken of selected grains and then later stitched together into one composite image (e.g., Fig. 9).

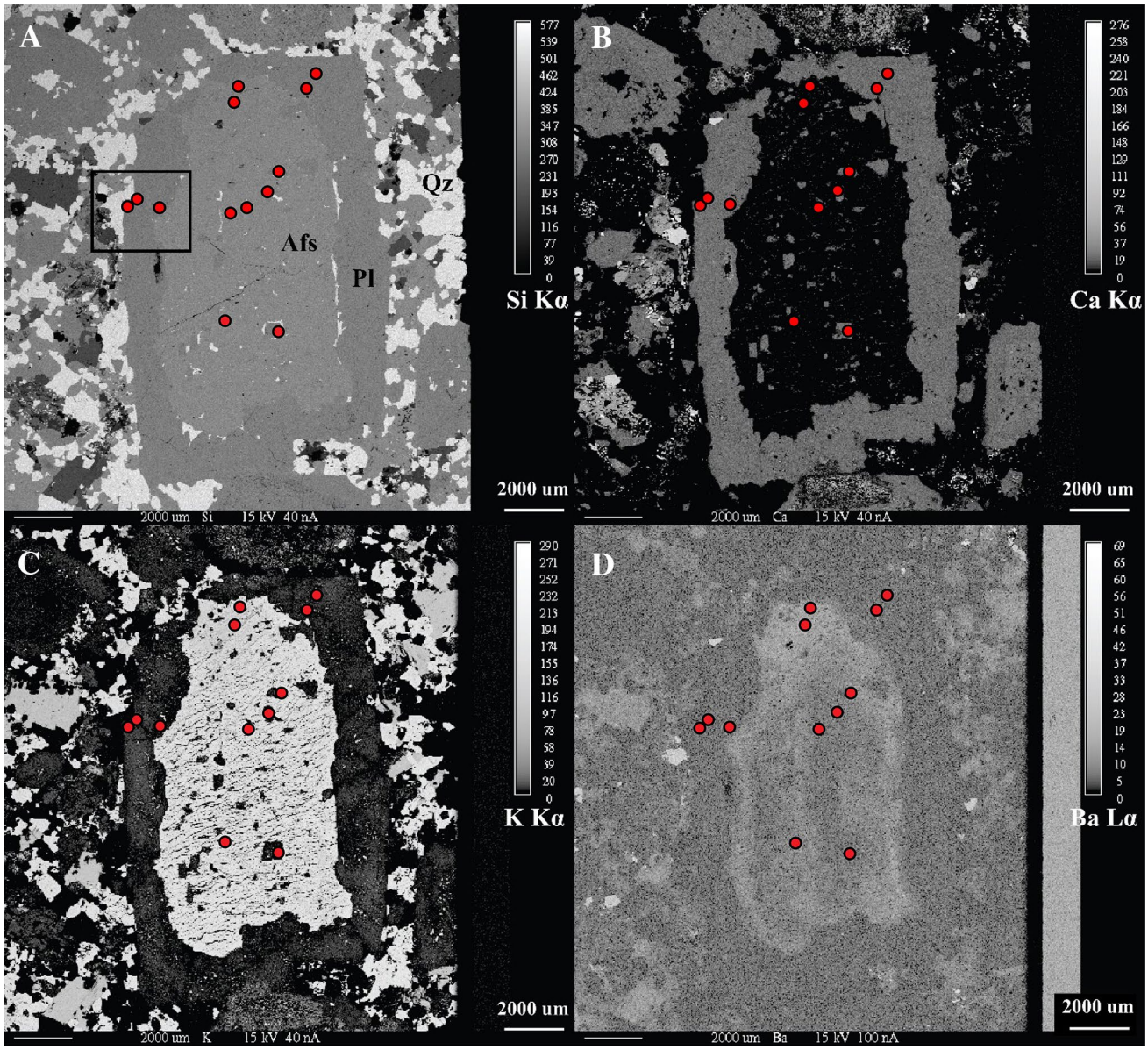

Fig. 3 X-ray-element maps of rapakivi grain FP-4-1R1. Greyscale-element maps of Si Kα (**a**), Ca Kα (**b**), K Kα (**c**), and Ba Lα (**d**) with Pb-isotope and trace-element analysis locations marked with red circles (size of circles greatly exaggerated in this and subsequent figures). Major phases are plagioclase (Pl), alkali feldspar (Afs), and quartz (Qz). Rectangle in **a** shows location of Fig. 15a

Results

Petrography

Rapakivi grains

Representative rapakivi feldspars from the Flye Point facies ranged from 1.5 to 2 cm across with generally tabular shapes reflective of their idiomorphic nature (Figs. 3, 4, 5, 6). Equant rapakivi grains were also present (Fig. 6) and are most likely due to their orientations during sectioning. The alkali feldspar cores are salmon in color and perthitic with a composition of about Or_{95} (Fig. 10). Contacts between the alkali feldspar cores and plagioclase mantles are generally irregular; however, euhedral faces developed on some alkali feldspar cores, where quartz forms a boundary between the mantle and core (Figs. 3a, 5a).

Mantling these alkali feldspar cores is at least one generation of plagioclase (~ An_{20}) up to 3 mm thick with its outermost edge being more albitic ($An_{8–14}$; Fig. 10). Plagioclase generally forms a complete mantle around a central alkali feldspar; however, partial mantling was seen in thin section and outcrop as well. Plagioclase is partly or completely optically continuous around the alkali feldspar cores. Simple

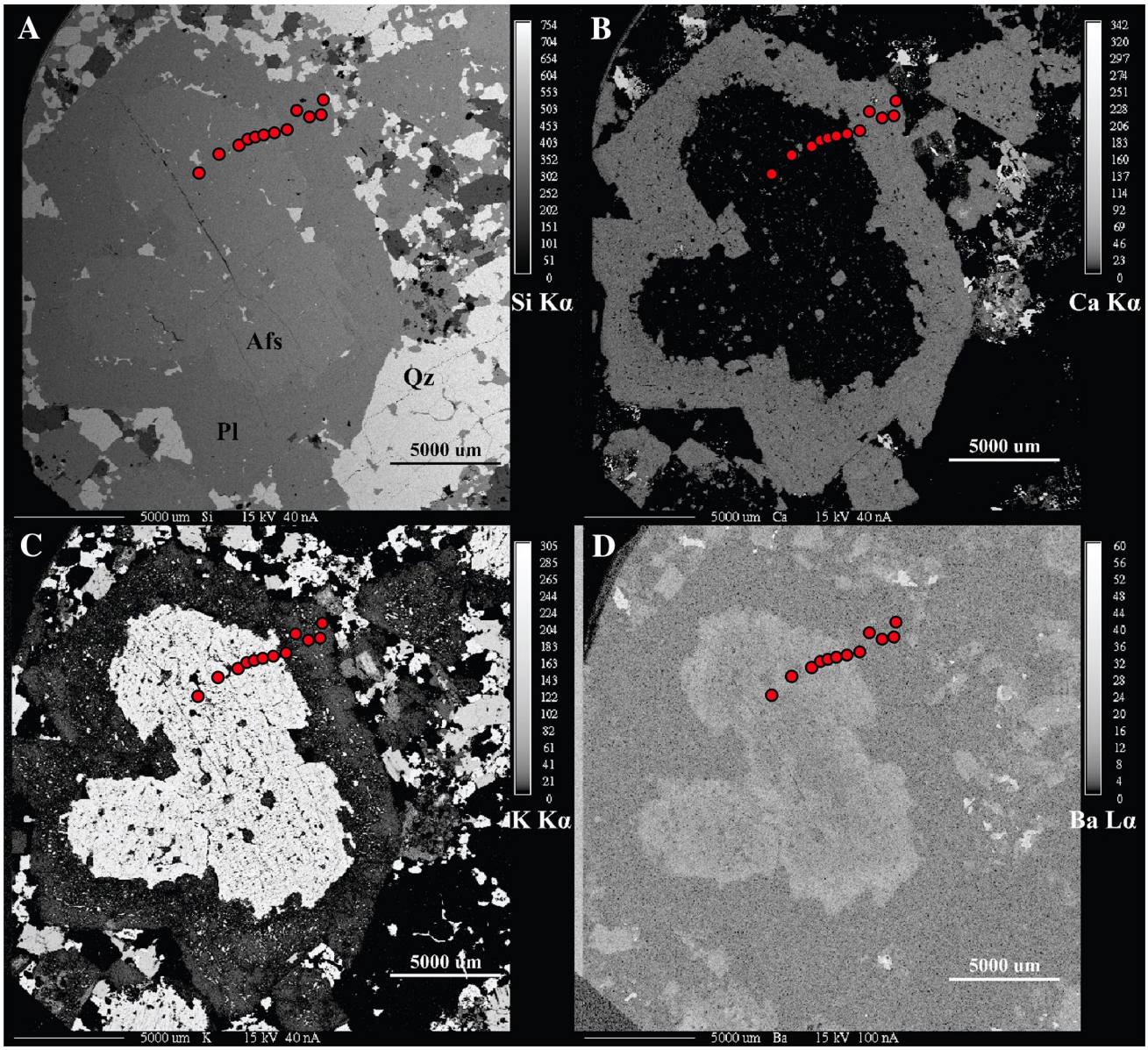

Fig. 4 X-ray-element maps of rapakivi grain FP-4-7R2. Greyscale-element maps of Si Kα (**a**), Ca Kα (**b**), K Kα (**c**), and Ba Lα (**d**) with Pb-isotope analysis locations marked with circles. Major phases include plagioclase (Pl), alkali feldspar (Afs), and quartz (Qz)

twins of alkali feldspar cores are continuous across core/mantle boundary and into the plagioclase mantle (cf. Vernon 2016). When multiple plagioclase mantles are present, some inner most mantles display a coarse-sieve texture (Fig. 5) and are compositionally similar to subsequent mantle generations ($An_{19–22}$; Fig. 10). Mantling by plagioclase, either by one or two generations, gives a subhedral to euhedral final shape to most grains.

Inclusions within the alkali feldspar cores are predominantly plagioclase. However, quartz, occasional biotite and apatite, and rare Fe–Ti oxides are also present in both cores and mantles. These inclusions are generally < 1 mm in size and occasionally are found in discrete zones that parallel primary growth zones within both alkali feldspar cores and plagioclase mantles. Plagioclase inclusions in the alkali feldspar cores are variably altered and dusty in thin section, and are generally more easily detected in Ca X-ray maps (Figs. 3, 4, 5, 6). Occasionally larger (~ 1 mm), and less altered, plagioclase inclusions are partially encased in quartz (Fig. 3). Rarely, plagioclase inclusions appear to be in optical continuity with the plagioclase in the mantle and may be re-entrants into the alkali feldspar core from the third dimension. For some rapakivi grains, quartz also forms thin pockets that separate plagioclase mantles from alkali feldspar cores and are usually optically continuous with other proximal quartz inclusions (Figs. 3, 4, 5). Where quartz is

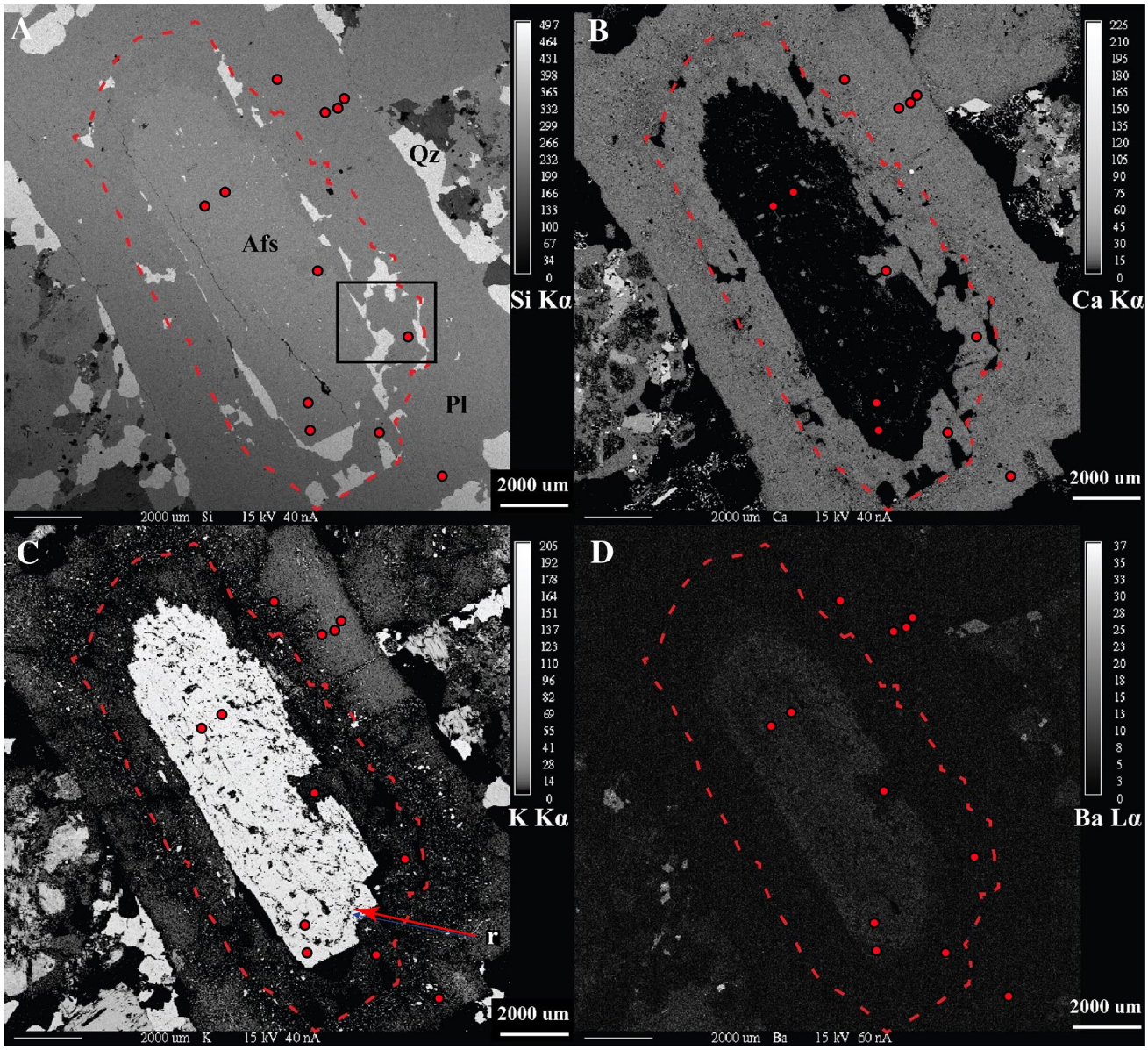

Fig. 5 X-ray-element maps of rapakivi grain FP-3-1R1. Greyscale-element maps of Si Kα (**a**), Ca Kα (**b**), K Kα (**c**), and Ba Lα (**d**) with Pb-isotope analysis locations marked with circles. Major phases included plagioclase (Pl), alkali feldspar (Afs), and quartz (Qz). Internal contact between inner, coarse-sieve-textured plagioclase mantle (first mantle) and outer, oscillatory zoned plagioclase mantle (second mantle) is marked by dashed line. Resorption surface (r) marked in **c**. Rectangle in **a** shows location of Fig. 15a

present, euhedral faces form on both alkali feldspar cores and plagioclase mantles (Fig. 5).

Plagioclase phenocrysts

Discrete phenocrysts of plagioclase feldspar are present; a minor population is mantled by a second generation of plagioclase. These generally larger phenocrysts are tabular and can be found up to 2.5 cm long (Fig. 7) and have cores of oligoclase (An_{23}–An_{27}: Fig. 10) that are slightly more calcic than the plagioclase mantles (~ An_{20}). The cores have coarse-sieve textures, much like the inner mantle of FP-3-1R1 (Fig. 5), with quartz infilling irregularly shaped voids [poikilitic grains of Lux et al. (2007)]. Also abundant in the cores are mafic silicate inclusions, typically biotite, with occasional amphibole, titanite, and Fe–Ti oxides. The plagioclase mantles are between 0.5 and 1.5 mm thick, generally pristine and inclusion-free and display minor oscillatory zoning. The outermost edge of these mantles is more albitic (~ An_{14}; Fig. 10) along the contact with matrix material, similar to that found on rapakivi feldspars.

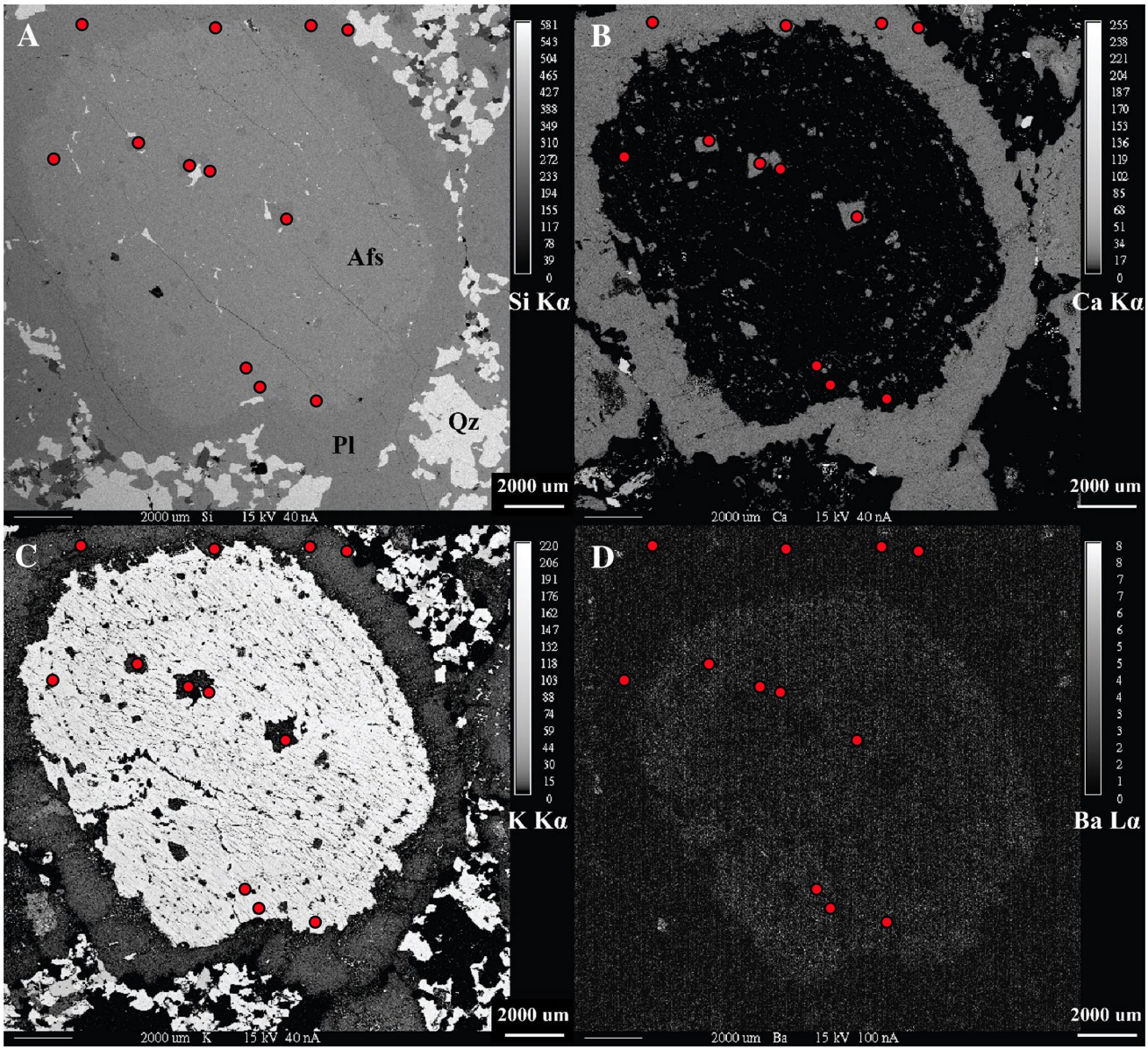

Fig. 6 X-ray-element maps of rapakivi grain FP-5-8R1. Greyscale-element maps of Si Kα (**a**), Ca Kα (**b**), K Kα (**c**), and Ba Lα (**d**) with Pb-isotope analysis locations marked with circles. Major phases include plagioclase (Pl), alkali feldspar (Afs), and quartz (Qz). Note the cyclic zoning of plagioclase inclusions easily seen in **b** and **c**

Alkali feldspar phenocrysts

Unmantled alkali feldspar grains up to 2 cm across are common in the Deer Isle Granite (Fig. 8). These grains are salmon colored and perthitic and typically display Carlsbad twinning. Internal oscillatory zoning is defined by variations in color from salmon pink to a more creamy pink. This appears to reflect changes in Ba concentrations as shown by the element maps (Fig. 8d). These alkali feldspar grains are typically mantled by a ~ 1 mm rim of Ba-rich (~ 0.7% BaO) alkali feldspar that formed after an inferred resorption event ("r" in Fig. 8d). Continued growth by Ba-poor alkali feldspar over Ba-rich mantle gives a subhedral appearance to most gains. Where Ba concentrations are relatively high, exsolution lamellae are less abundant compared to other parts of the grain (Fig. 8).

Quartz phenocrysts

Quartz phenocrysts are found as much as 1 cm across forming anhedral to subhedral, poorly rounded to rounded grains. Grains are seen as either amalgamations of several distinct crystals, with generally a central or dominant crystal making up the majority of the cluster, or as single distinct grains

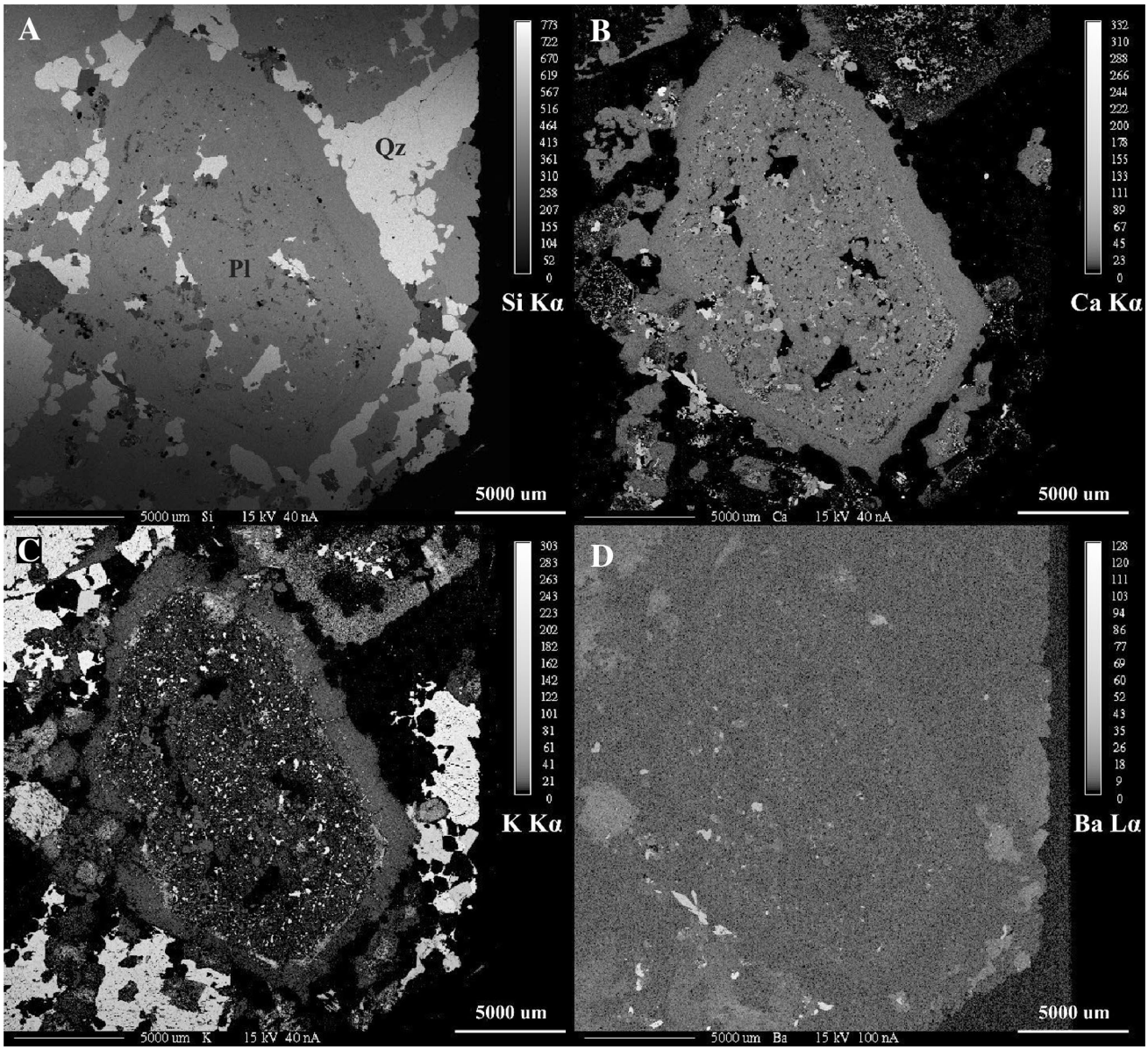

Fig. 7 X-ray-element maps of plagioclase phenocryst FP-6-1P1. Greyscale-element maps of Si Kα (**a**), Ca Kα (**b**), K Kα (**c**), and Ba Lα (**d**). Major phases present are plagioclase (Pl) and quartz (Qz)

(Fig. 9). Cathodoluminescence (CL) imagery of several quartz grains revealed primary growth zonation that includes normal (bright to dark) and reverse (dark to light) step zoning (Fig. 9); zoning trends are based on the assumption that the brighter zones are richer in Ti and crystallized at higher temperatures than the lighter ones (e.g., Müller et al. 2005). Quartz grains exhibiting distinct oscillatory zoning have successions of brighter and darker growth domains around central cores. These domains generally exhibit euhedral crystal habits that are accentuated by normal and reverse zoning. Contacts are sharp and irregular with newer domains truncating older ones along an inferred resorption surface (arrows in Fig. 9). The last quartz to mantle these phenocrysts generally exhibit a darker luminescence than that seen internally and produces an anhedral texture.

Secondary features found in all CL images of quartz are fine, dark, wispy bands that appear to represent healed brittle fractures ("f" in Fig. 9). These are over printed by nearly non-luminescence quartz that surrounds fluid inclusions giving the appearance of dark fractures to the images ("i" in Fig. 9).

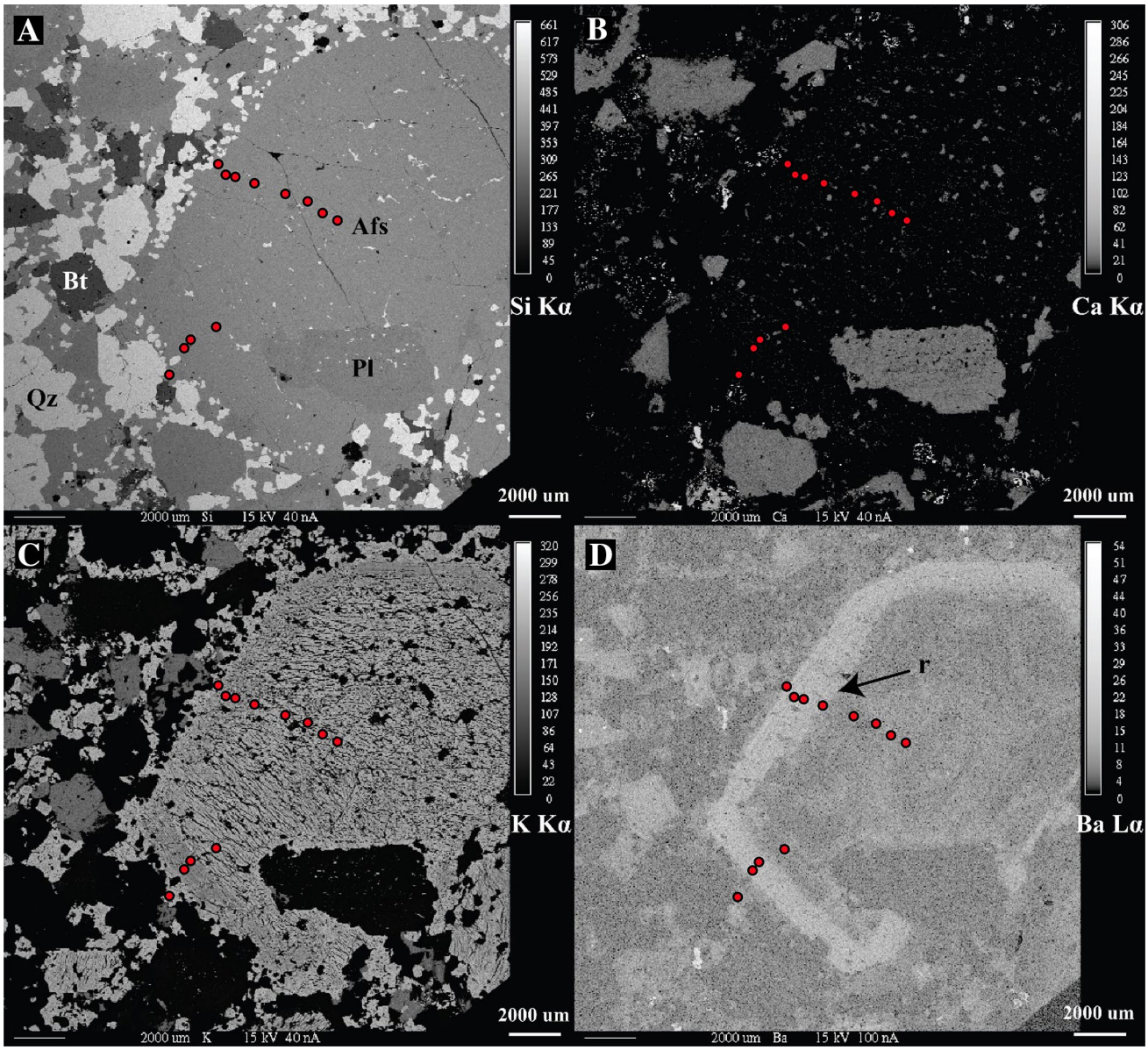

Fig. 8 X-ray-element maps of unmantled alkali feldspar phenocryst FP-4-7R1. Greyscale-element maps of Si Kα (**a**), Ca Kα (**b**), K Kα (**c**), and Ba Lα (**d**) with Pb-isotope analysis locations marked with red circles. Major phases include plagioclase (Pl), alkali feldspar (Afs), quartz (Qz), and biotite (Bt). Perthitic nature of alkali feldspar is clearly seen in K map **c**. Ba-rich zone is easily seen in Ba map 8D and highlights an inferred resorption surface (r), marked by arrow

Feldspar chemistry

Major elements

For all alkali feldspar cores, compositions typically varied between Or_{90} and Or_{97} (Fig. 10). Rimward towards the core–mantle boundary, Ba concentrations are typically higher (> 0.3% BaO) relative to the inner core zones (~ 0.1% BaO) (e.g., FP-4-7R2, Fig. 4d). In these Ba-rich zones, Or is generally much lower and exhibits a larger degree of variability (Or_{62}–Or_{90}). Perthitic and microperthitic textures are present in all samples with lamellae ranging from 91 to 99 mol % Ab (Fig. 10). Perthite is less developed in areas of the cores, where the BaO concentration is higher (> 0.5 wt%) and is believed to be the reason for the lower mol % Or values noted above. Higher BaO content must have inhibited albite exsolution from the alkali feldspar.

Plagioclase phenocrysts are the most An rich with cores of up to An_{27} (Fig. 10) Plagioclase mantles, on both plagioclase phenocrysts and rapakivi grains, have a mean composition of An_{20} and are typically oscillatory zoned with maximum amplitudes of 3 mol % An. Albitic plagioclase

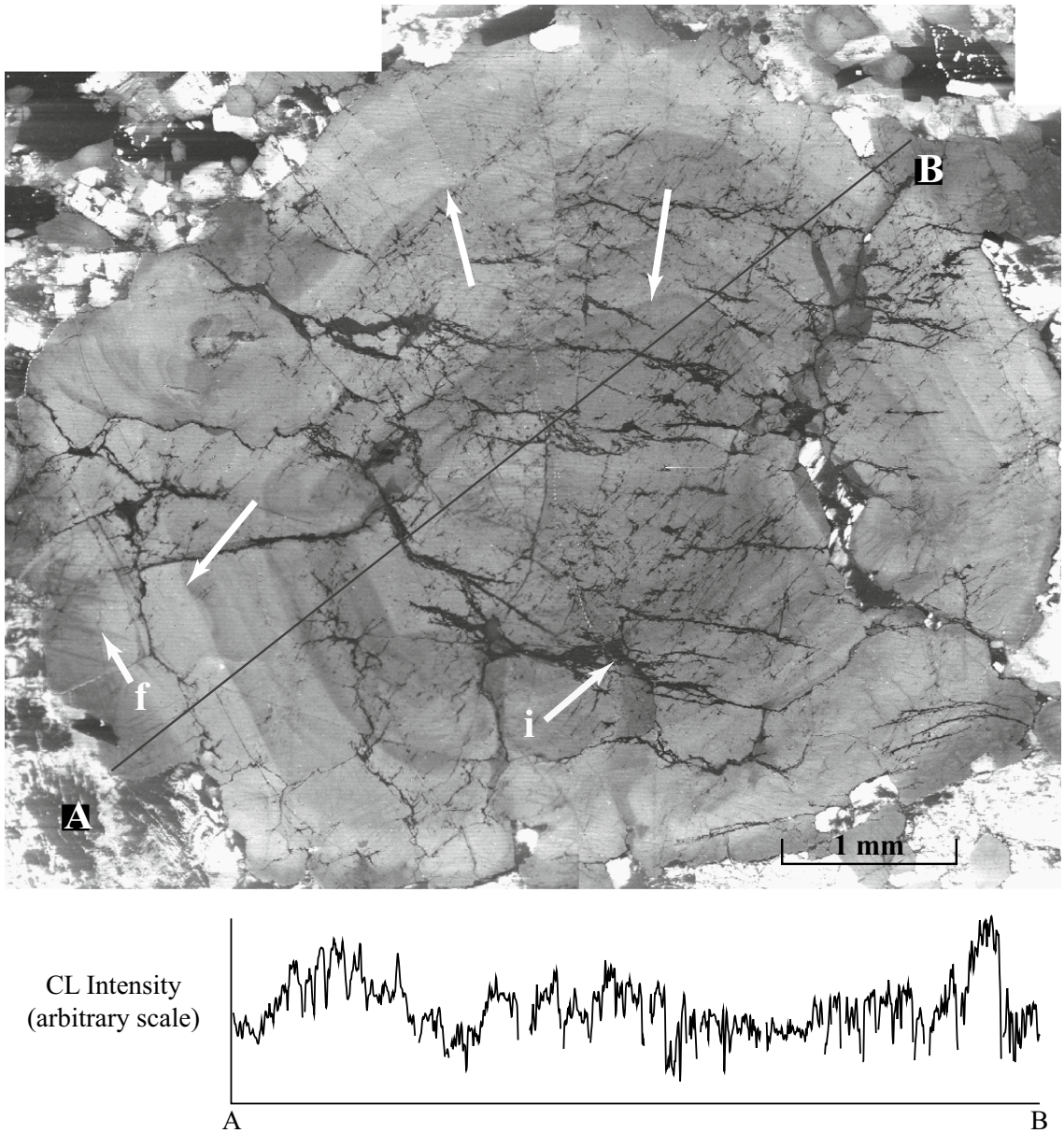

Fig. 9 Cathodoluminescence image of quartz phenocryst from the Flye Point facies (FP-5-6) showing distinct bright growth zones, an inferred response to changing temperature or Ti concentrations. Brittle fractures (f) and fluid inclusions (i) are present throughout. White arrows mark resorption surfaces that have been over grown by more luminescent quartz (note truncated zone below left most arrow). Line represents transect across phenocryst, which is shown below. Gaps in profile represent, where transect intersected fluid inclusion-rich zones

($An_{<14}$) forms the outermost edge on both rapakivi and plagioclase phenocrysts. Plagioclase inclusions within alkali feldspar cores of rapakivi grains have a mean value of An_{20} and, like the mantles, have more albitic rims (An_{13}). Within the coarse-sieve textured regions of both plagioclase phenocrysts (Fig. 7) and double-mantled rapakivi feldspars (Fig. 5), albitic plagioclase ($An_{14–17}$) is found along contacts with quartz pockets. Isolated albitic patches are also noted within this region and may represent the same contact with quartz, only in the third dimension.

Or contents of the plagioclase phenocryst cores are relatively low compared to their mantles—indicating either a lower temperature of crystallization or more advance low T re-equilibration. Likewise, the plagioclase in rapakivi mantles has higher or than that in the inner mantles (Fig. 10).

Trace elements

Trace-element analyses by LA-ICP-MS (Figs. 11, 12, 13, 14) were conducted on plagioclase mantles of rapakivi grains,

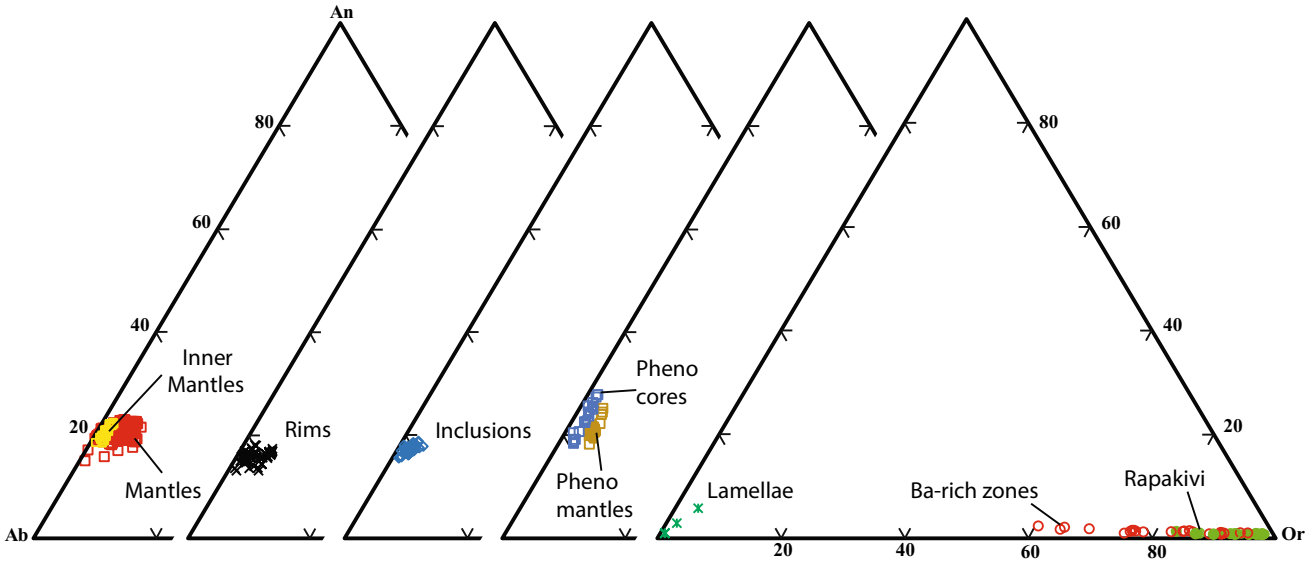

Fig. 10 Feldspar ternary diagram with compositions of rapakivi cores (alkali feldspar), mantles (plagioclase), plagioclase phenocrysts, and alkali feldspar phenocrysts from the Flye Point facies of the Deer Isle Granite Complex

plagioclase inclusions in the alkali feldspar cores, and plagioclase phenocrysts. Alkali feldspar cores and phenocrysts were not analyzed using LA-ICP-MS so comparisons of rapakivi alkali feldspar cores and alkali feldspar phenocrysts were done using major element (including Ba) maps (Figs. 3, 4, 5, 6, 7, 8) and spot analyses with the electron microprobe (Supplementary Table 1). Below, we describe the elemental variations in 5 grains from 3 hand samples of the Flye Point facies of the Deer Isle Granite Complex.

Rapakivi FP-4-1R1 Trace-element concentrations in rapakivi grain FP-4-1R1 (element maps are portrayed in Fig. 3) are presented in Fig. 11a–c. Plagioclase inclusions within the Ba-poor alkali feldspar core have lower concentrations of Ba, La, and Ce than plagioclase in the mantle. This lower concentration is independent of An content, since both plagioclase inclusions and plagioclase mantles are ~ An_{20} (Fig. 10).

Variations in trace-element concentrations, seen especially in Ba (Fig. 11a), indicate oscillatory zoning of the plagioclase mantle. This oscillatory zoning is also visible in CL images of the rapakivi grain (Fig. 15a). La and Ce concentrations show similar, but more subdued, variations; Ba concentrations in the feldspars appear to be more sensitive to changes in melt composition than La or Ce, probably because of the much higher partition coefficients for Ba in plagioclase than for the LREE (e.g., Dailey et al. 2018).

Rapakivi FP-4-7R2 The relatively small size and minor alteration of plagioclase inclusions within the alkali feldspar core of rapakivi grain FP-4-7R2 deterred their analysis; however, it is noted that a plagioclase-rich zone of inclusions is discernible in element maps (Fig. 4). A Ba-rich zone within the outer part of the alkali feldspar core is also observed in element maps (Fig. 4d) and has been marked in Fig. 12.

Within the plagioclase mantle of the composite grain, Ba, La, and Ce concentrations are relatively low along the core–mantle boundary (Fig. 12a–c). In addition, within this zone, the An content is atypically lower ($An_{18–19}$) than that found in the rest of the mantle ($An_{20–22}$). Rimward, distinctive increases in Ba and LREE concentrations occur, such that a double mantle is evident. Most notably, Ba concentrations double from ~ 150 to 300 ppm (Fig. 12a), something not evident in the element map (Fig. 4d). For Ba, this increase in concentration is then followed by an abrupt decrease to values comparable to those along the core–mantle boundary (~ 150 ppm). La and Ce concentrations form similar patterns of low, high, and low concentrations rimward in the mantle. However, the outer zone of relatively low concentrations of LREE is on average slightly higher than those along the core–mantle boundary (Fig. 12b, c). Rimward from the core–mantle boundary zone, where Ba, La, and Ce increase, the subsequent increase and then decrease in trace-element concentrations, is not accompanied by a change in An concentrations and values remain consistently ~ An_{21}.

Rapakivi FP-3-1R1 A texturally distinct, double mantle of plagioclase on this rapakivi grain is seen optically and in X-ray-element maps (Fig. 5). Much like FP4-7R2, Ba, La, and Ce concentrations are relatively low within the inner most part of the coarse-sieve textured plagioclase mantle

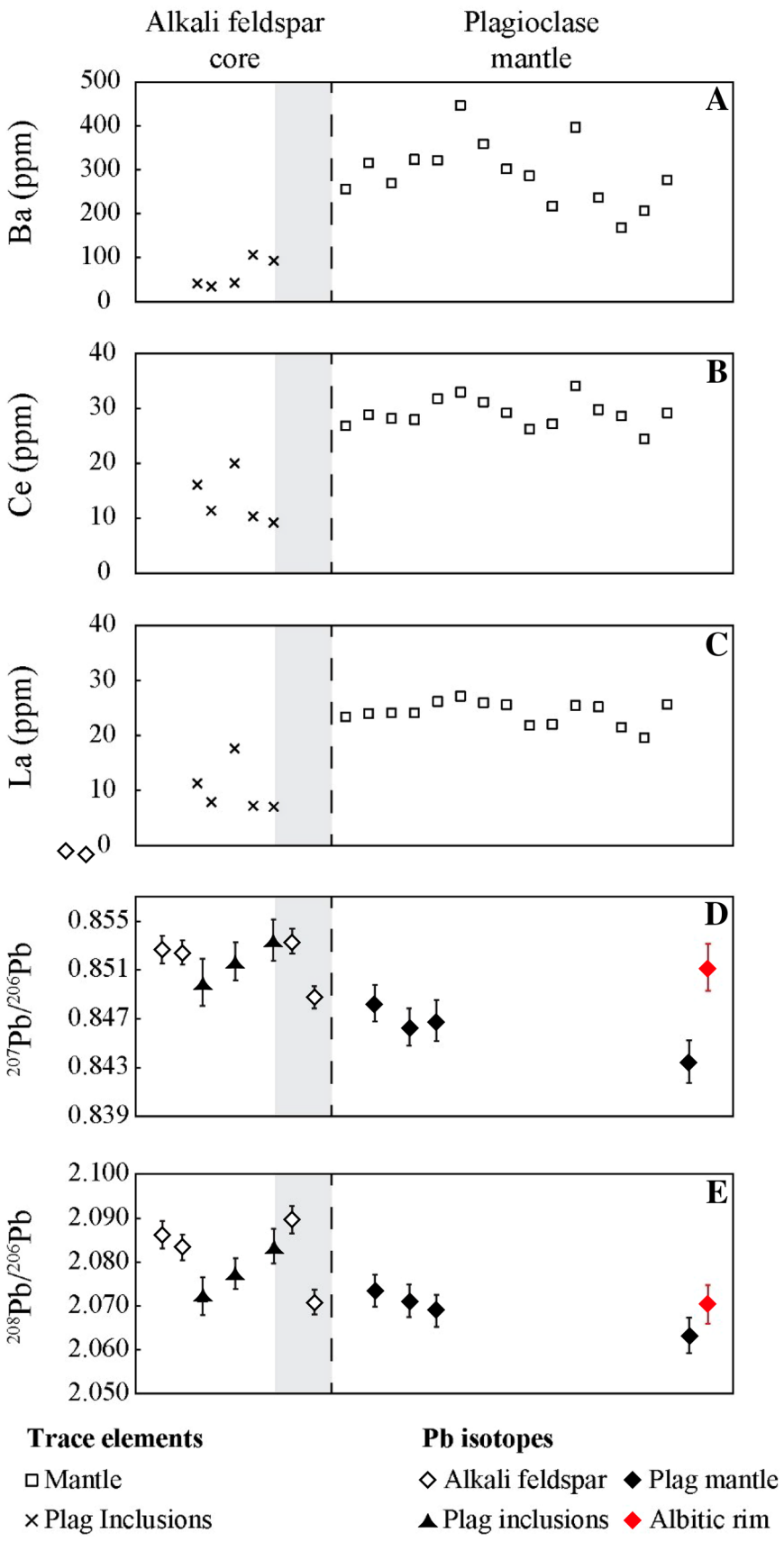

Fig. 11 Trace element and Pb-isotope core to rim profiles of rapakivi grain FP-4-1R1 and its plagioclase inclusions (X-ray-element images shown in Fig. 3). Bold dashed line represents core–mantle boundary (alkali feldspar–plagioclase contact) within grain. Gray area marks Ba-rich alkali feldspar zone revealed in Ba-element map (Fig. 3d). Trace-element uncertainties are smaller than symbols and Pb-isotope ratio uncertainties show 2σ error bars

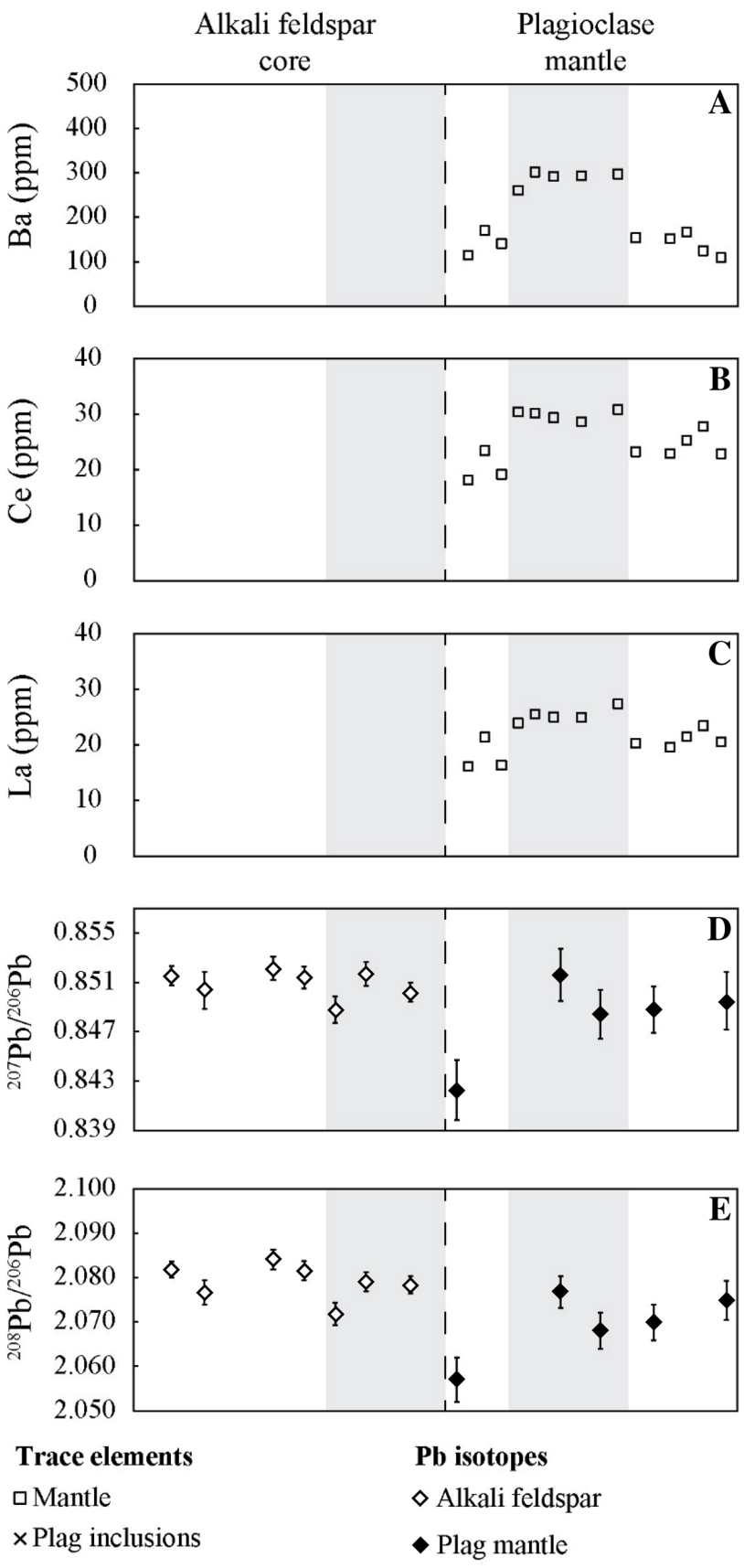

Fig. 12 Trace element and Pb-isotope core to rim profiles of rapakivi grain FP-4-7R2 (X-ray-element images shown in Fig. 4). Bold dashed line represents core–mantle boundary (alkali feldspar–plagioclase contact) within grain. Gray areas mark zones of Ba-rich alkali feldspar (core) and plagioclase (mantle) within grain. Trace-element errors are smaller than symbol and Pb-isotope uncertainties show 2σ error bars

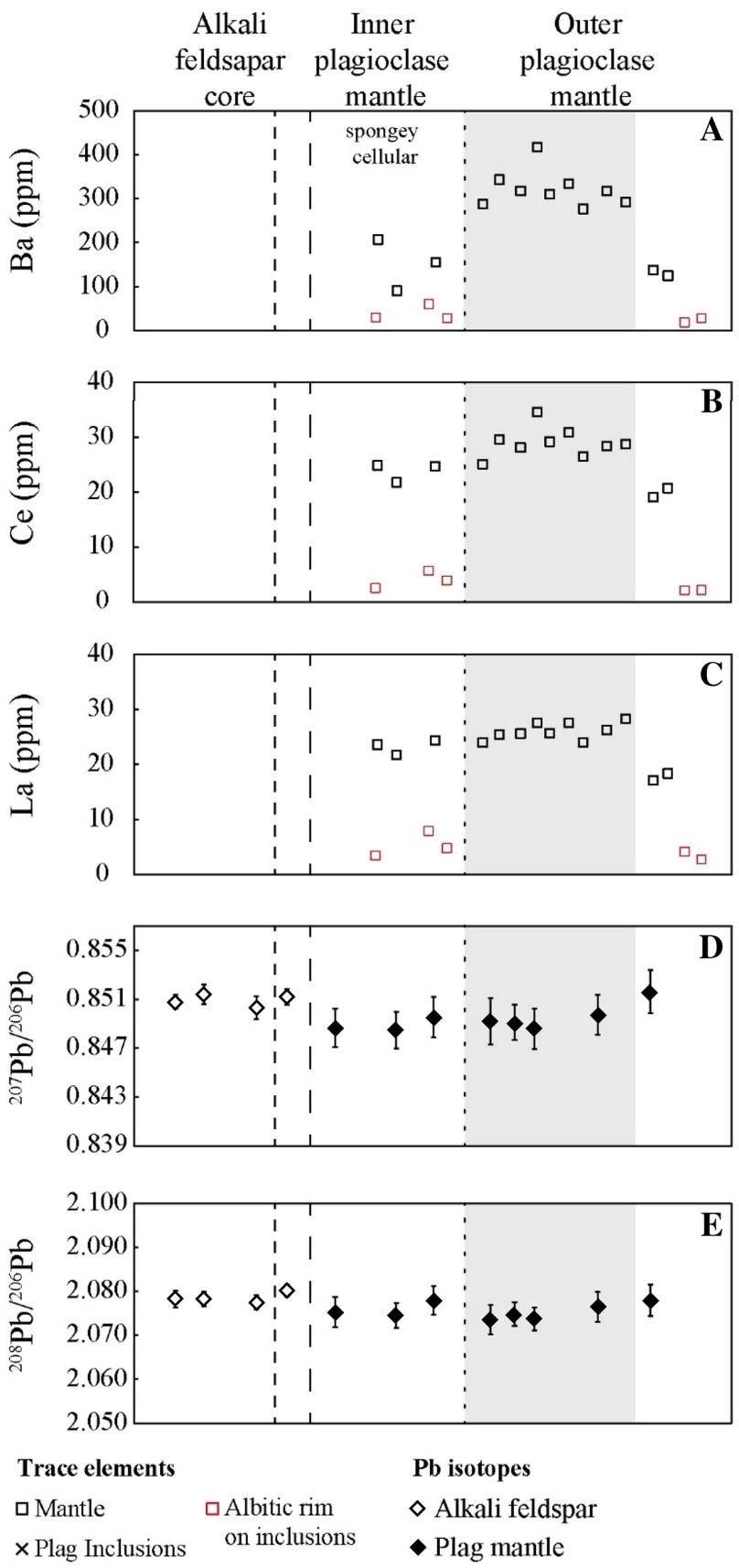

Fig. 13 Trace element and Pb-isotope core to rim profiles of rapakivi grain FP-3-1R1 (X-ray-element images shown in Fig. 5). Bold dashed line represents core–mantle boundary (alkali feldspar–plagioclase contact) within grain. Dashed line represents resorption surface (r) in Fig. 5c. Dotted line represents contact between the first and second plagioclase mantles. Gray areas mark zone of Ba-rich plagioclase within mantle. Trace-element errors are smaller than symbol and Pb-isotope uncertainties show 2σ error bars

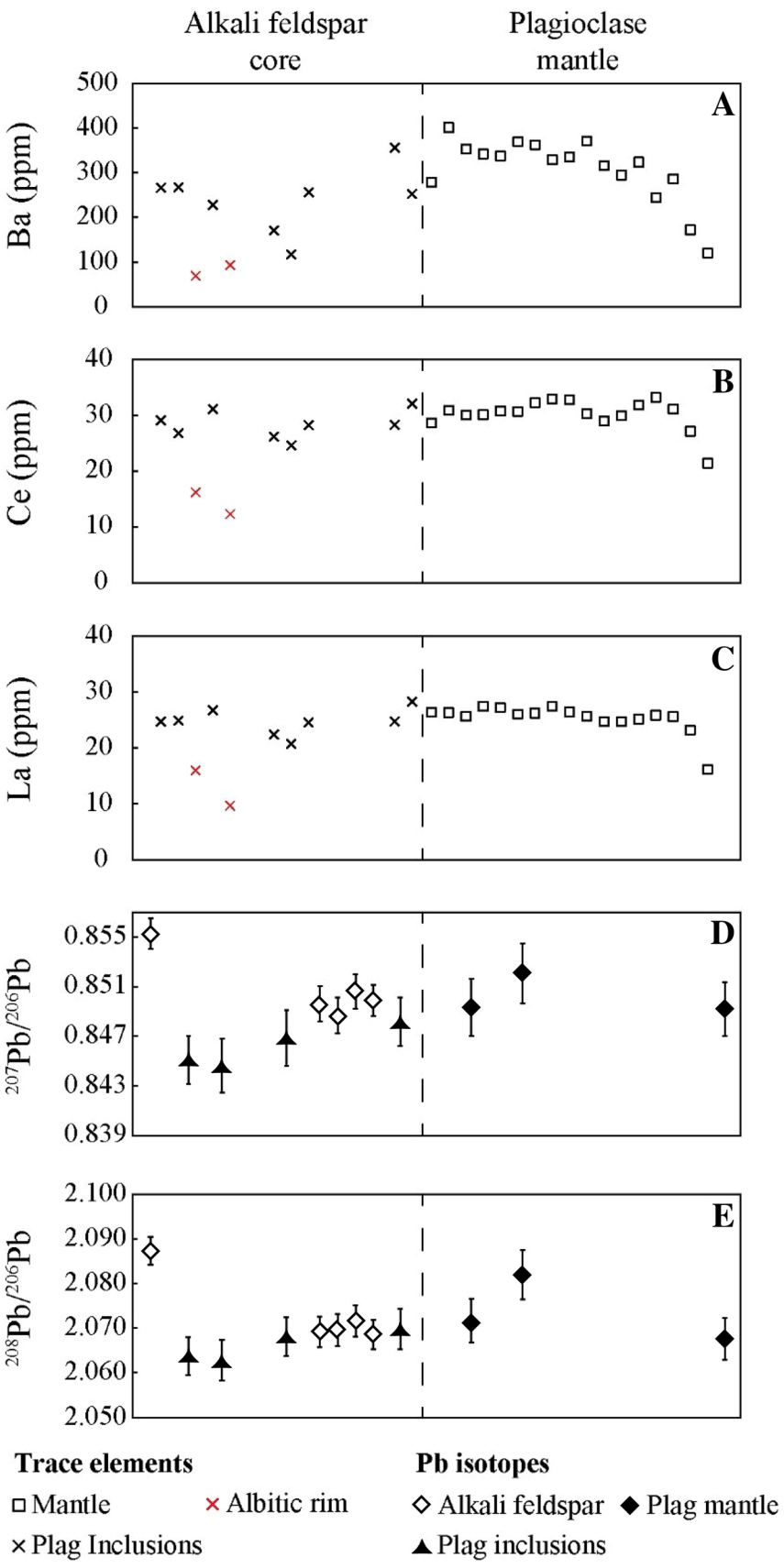

Fig. 14 Trace element and Pb-isotope core to rim profiles of rapakivi grain FP-5-8R1 (X-ray-element images shown in Fig. 6). Bold dashed line represents core–mantle boundary (alkali feldspar–plagioclase contact) within grain. Trace-element errors are smaller than symbol and Pb-isotope uncertainties show 2σ error bars

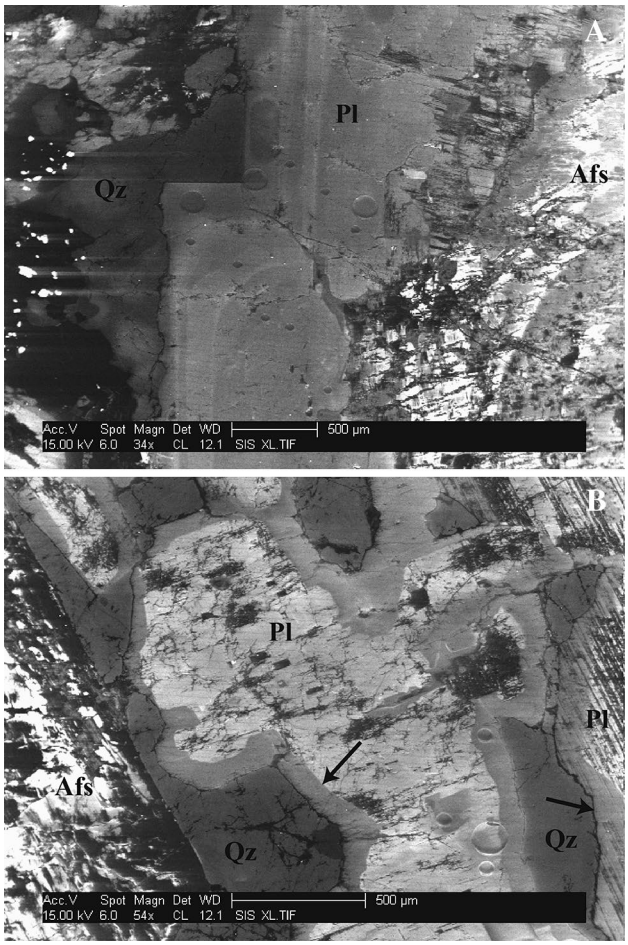

Fig. 15 **a** CL image showing oscillatory zoning in plagioclase mantle (Pl) and in the alkali feldspar core (Afs) of rapakivi grain FP-4-1R1 (see Fig. 3 for location). Note subhedral/euhedral plagioclase growth where in contact with quartz (Qz). Relative brighter regions indicate increases in either rare earth elements (e.g., Ce^{3+} or Eu^{3+}) or defects in crystal lattice that may be due to ion substitutions (e.g., Al^{3+} for Si^{4+}) [Boggs and Krinsley (2006) and citations within]. **b** CL image showing coarse-sieve texture of the first plagioclase mantle in rapakivi grain FP-3-1R1 (see Fig. 6 for location). Note the euhedral face of alkali feldspar core (Afs) in contact with quartz (Qz). Plagioclase (Pl) of both the coarse-sieve textured first (center) and second (far right) mantle shows growth of more albitic phase (arrows), where it is in contact with quartz

(Fig. 13a–c). Rimward, concentrations of these incompatible trace elements increase and then decrease in the outer part of the plagioclase mantle. As in FP-4-7R2, the changes are most notably seen in Ba concentrations. Within the inner mantle, values average ~ 150 ppm for Ba (Fig. 13a). Ba concentrations more than double to about ~ 320 ppm in a zone also enriched in La and Ce. The punctuated decrease in Ba, La, and Ce concentrations within the outer part of the second plagioclase mantle is nearly identical to that seen in the mantle of FP-4-7R2. The albitic zones have low Ba, La, and Ce concentrations.

Ba, La, and Ce are all strongly depleted along the most outer edge of the outer mantle, where plagioclase also becomes more albitic (~ An_{14}). The declining An, Ba, La, and Ce are again most likely due to fractionation of the host magma with the continued growth of quartz, plagioclase, alkali feldspar, and the accessory phases allanite and titanite. Albitic rims of plagioclase in contact with quartz are also found within the coarse-sieve textured area of the inner mantle (Figs. 5, 15b). These albitic rims may reflect continued feldspar growth accompanying fractionation of trapped melt, or more likely, subsolidus growth during the exsolution of alkali feldspar. Due to their small sizes, plagioclase inclusions within the alkali feldspar core were not analyzed.

Rapakivi FP-5-8R1 Although not as pronounced as in some of the previously described grains, the alkali feldspar core of rapakivi grain FP-5-8R1 has a zone of plagioclase inclusions near its outer edge (Fig. 6). The Ba concentrations in these outermost inclusions are, on average, higher than concentrations in inclusions found farther in the core of the rapakivi grain FP-5-8R1 (Fig. 14). No major changes in La and Ce concentrations are observed in plagioclase inclusions across the alkali feldspar core. Ba, however, may form a fractionation trend (decreasing from 267 ppm to 117 ppm) within the inner half of the core. This decrease is followed by a jump back to ~ 250 ppm Ba in plagioclase inclusions in the outer part of the core. Trace-element (Ba, La, and Ce) concentrations within albitic rims of plagioclase inclusions were the lowest observed.

In the plagioclase mantle, trace-element concentrations are relatively constant for over half the width of the mantle, after which a distinct fractionation trend is observed with declining Ba, La, and Ce. It is noted that oscillatory zones seen optically in the plagioclase mantle are very narrow (< 50 µm). This caused spatial resolution issues with analyses as a single laser spot (50 µm) sometimes sampled two-to-three oscillatory zones at once and so provided more of an average over the area analyzed. This could have averaged any variations in trace-element concentrations caused by the oscillatory zoning.

Alkali feldspar phenocryst FP-4-7R1 Although LA-ICP-MS trace-element analyses were not conducted on this alkali feldspar phenocryst, BaO was analyzed by electron microprobe (Supplementary Table 1). Due to the observed correlation of Ba–La and Ce in other grains, the Ba data are used here for comparison. The core of this alkali feldspar grain has an average BaO concentration of ~ 0.1 wt% with only minor zoning seen in the element map (Fig. 8d). A resorption surface (r in Fig. 8d) marks the boundary between a Ba-poor core and a 2 mm wide Ba-rich rim. This rim has oscillatory zoning with an average BaO concentration of

0.51 wt%, with concentrations reaching as high as 0.79 wt% (Fig. 8; Supplementary Table 1).

Pb isotopes

Rapakivi FP-4-1R1 The inner, Ba-poor alkali feldspar core of this rapakivi grain (Fig. 3) has average $^{207}Pb/^{206}Pb$ of ~ 0.853 and $^{208}Pb/^{206}Pb$ of ~ 2.085 (Fig. 11d, e). Plagioclase inclusions within the innermost Ba-LREE-poor core have a slightly lower isotopic signature ($^{207}Pb/^{206}Pb = 0.850$ and $^{208}Pb/^{206}Pb = 2.072$), but then trend back to values similar to those in the innermost area of the alkali feldspar core. The most rimward plagioclase inclusion falls along the contact, where the Ba-poor alkali feldspar core is overgrown by a more Ba-rich alkali feldspar. Isotopic ratios within this inclusion and those within the Ba-rich plagioclase overgrowth are comparable to each other ($^{207}Pb/^{206}Pb = 0.848$ and $^{208}Pb/^{206}Pb = 2.071$; Fig. 11d, e).

Across the core–mantle boundary, isotopic values continue to drop rimward to the lowest values found within the grain ($^{207}Pb/^{206}Pb = 0.843$ and $^{208}Pb/^{206}Pb = 2.063$). Along the most outer more albitic edge of the mantle (which is marked by a decrease in mol % An–An_{15}), Pb-isotopic ratios increase ($^{207}Pb/^{206}Pb = 0.851$ and $^{208}Pb/^{206}Pb = 2.070$).

Rapakivi FP-4-7R2 Like FP-3-1R1, this grain also has a relatively Ba-poor alkali feldspar inner core that is overgrown by more Ba-rich alkali feldspar (Fig. 4). Within the Ba-poor inner core, there is a slight variation in the Pb-isotope ratios (Fig. 12d, e) that show two minor steps, where there is a slight drop in isotopic ratios. The second of these minor drops is located near the contact between the Ba-poor and Ba-rich alkali feldspar core. Outward from here, across the more Ba-rich alkali feldspar to the core–mantle boundary, ratios return to the slightly higher values of the inner core.

Outside of the core, the isotopic ratios in the plagioclase mantle drop to the lowest values seen in any of the analyzed grains ($^{207}Pb/^{206}Pb = 0.842$ and $^{208}Pb/^{206}Pb = 2.057$). As stated above, Ba, La, and Ce are also depleted within this mantle.

Rimward, within a Ba-rich zone (Fig. 12a) of the plagioclase, Pb-isotope ratios jump to values similar to those in the alkali feldspar core ($^{207}Pb/^{206}Pb = 0.852$ and $^{208}Pb/^{206}Pb = 2.077$), but then drop to relative moderate values ($^{207}Pb/^{206}Pb = 0.848$ and $^{208}Pb/^{206}Pb = 2.068$). From here, and within another zone of depleted Ba, La, and Ce, Pb-isotopic ratios gently increase rimward (Fig. 12d, e).

Rapakivi FP-3-1R1 As shown in Fig. 5, this rapakivi grain has a double plagioclase mantle with the inner mantle possessing a coarse-sieve texture and the outer mantle showing typical oscillatory zoning.

Within the alkali feldspar core, the Pb-isotopic ratios are essentially constant and similar to those in other grains ($^{207}Pb/^{206}Pb = 0.851$ and $^{208}Pb/^{206}Pb = 2.079$ (Fig. 13d, e). Unique to this grain is an inferred resorption surface within the outer edge (near the core–mantle boundary) of the core ("r" in Fig. 5c and shorter dashed line in Fig. 13). Only a slight increase in $^{208}Pb/^{206}Pb$ ratios exists between the inner and outer (after resorption surface) cores, but this difference is within error of the other analyses (Fig. 13e).

A minor decrease in Pb-isotopic ratios occurs with the transition across the core–mantle boundary into the first plagioclase mantle. Within this innermost Pl mantle, $^{207}Pb/^{206}Pb$ values average 0.849 and $^{208}Pb/^{206}Pb$ values average 2.076. Ratios within the second plagioclase mantle also show limited variability with an average of 0.849 and 2.074 for $^{207}Pb/^{206}Pb$ and $^{208}Pb/^{206}Pb$, respectively. The three outermost analyses indicate a trend of increasing Pb-isotopic ratios that match the values of the alkali feldspar core.

Rapakivi FP-5-8R1 Unlike other rapakivi gains, FP-5-8R1 displays a distinct ovoidal morphology, possibly caused by sectioning perpendicular to the *c*-axis (Fig. 6). The innermost alkali feldspar analysis has the highest Pb-isotope ratios (Fig. 14d, e) measured in any of the alkali feldspar cores ($^{207}Pb/^{206}Pb = 0.855$ and $^{208}Pb/^{206}Pb = 2.087$). Rimward, to the zonally (crystallographically) arranged euhedral plagioclase inclusions, there is a large decrease in isotopic ratios ($^{207}Pb/^{206}Pb = 0.845$ and $^{208}Pb/^{206}Pb = 2.064$) (Fig. 14d, e). Pb-isotopic values within these plagioclase inclusions increase slightly towards the core–mantle boundary. Average ratios of 0.849 and 2.070 ($^{207}Pb/^{206}Pb$ and $^{208}Pb/^{206}Pb$, respectively) for the outer part of the alkali feldspar core appear to lie along the trend defined by the plagioclase inclusions.

Within the plagioclase mantle, Pb-isotope ratios closest to the core–mantle boundary appear to be the same as those found in the outer core. The centermost analysis of the plagioclase mantle shows a minor increase in Pb-isotopic ratios with no associated change in Ba, La, or Ce concentrations or An content. It is noted again that the width of the oscillatory zones was < 50 µm for some areas of the mantle and caused spatial resolution issues (laser spot size = 50 µm).

Following this increase, isotopic ratios drop to values comparable to the outer core average ($^{207}Pb/^{206}Pb = 0.849$ and $^{208}Pb/^{206}Pb = 2.068$) (Fig. 14).

Alkali feldspar phenocryst FP-4-7R1 Although not a rapakivi, this alkali feldspar phenocryst displays an inner core that has been overgrown by a rim of Ba-rich alkali feldspar (Fig. 8). Much like the rapakivi feldspars, the inner alkali feldspar core has average Pb-isotope ratios of 0.851 and 2.090 ($^{207}Pb/^{206}Pb$ and $^{208}Pb/^{206}Pb$, respectively; Fig. 16). These ratios decrease markedly near the contact with the

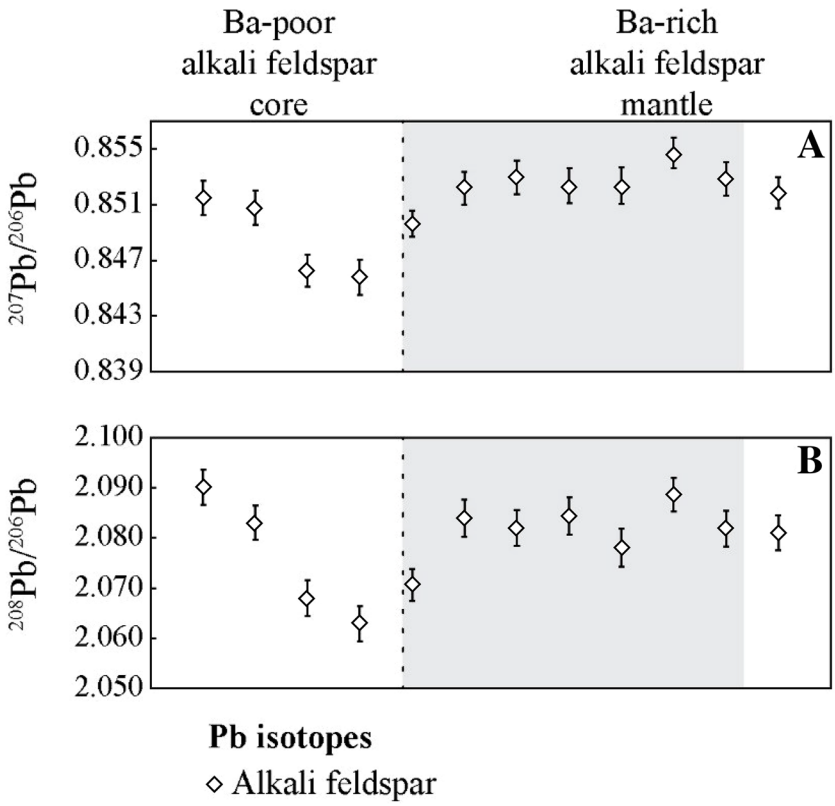

Fig. 16 Pb-isotope core to rim profiles of alkali feldspar grain FP-4-7R1. Dashed line marks contact between Ba-poor inner core and Ba-rich rim (gray area). Pb-isotope uncertainties show 2σ error bars

Ba-rich rim. Crossing the boundary, this drop is followed by the increase of Pb-isotope ratios back to values similar to the inner core ($^{207}Pb/^{206}Pb = 0.852$ and $^{208}Pb/^{206}Pb = 2.084$).

Discussion

As noted in the introduction, the formation of rapakivi feldspars has been explained by crystallization during isothermal decompression of granitic magma (e.g., Nekvasil 1991; Eklund and Shebanov 1999), by magma mixing (e.g., Wark and Stimac 1992), and by subsolidus alteration (Dempster et al. 1994; Mondal et al. 2017). In the case of the Deer Isle pluton, we think that a subsolidus alteration model is not applicable for two main reasons. First, the plagioclase mantles commonly display oscillatory zoning, a type of zoning attributed to magmatic processes, not subsolidus ones (Hibbard 1994). Second, thin wisps of albite coat oligoclase; these we interpret to be subsolidus in origin formed as the plagioclase mantle experienced exsolution of Ab. These coatings display distinct Ba, La, and Ce concentrations (Figs. 13, 14) compared to the oligoclase inclusions in alkali feldspar and rapakivi mantles that we interpret to be magmatic. We, therefore, focus on the decompression and magma-mixing origins of rapakivi.

To review, isothermal decompression of a granitic magma has been shown to cause alkali feldspar and quartz to become unstable, while plagioclase remains stable (e.g., Nekvasil 1991). During ascent, the resorbed alkali feldspar provides the nuclei for additional growth of plagioclase. Because there is no contamination of the host magma, isothermal decompression is considered a closed system hypothesis. Magma mixing, on the other hand, represents an open system. Here, the host magma is contaminated by another magma (or magmas) during crystallization. If crystallization of alkali feldspar has occurred in the host magma when mixing begins, the injection of a hotter, and/or chemically different, magma could destabilize Qz and Afs in the host and cause resorption of both phases. As cooling (equilibration) again begins, these partially resorbed alkali feldspars act as nucleation surfaces for plagioclase.

In a closed system, because there are no external inputs into the magma system, the host magma's Pb-isotopic composition will not change during crystallization. Thus, minerals that crystallized prior to decompression will have the same isotopic signatures as those that formed after ascent and emplacement of the magma. In an open system, the host magma's bulk chemistry may be changed with the subsequent addition of new batches of magma. The resulting minerals may, therefore, show trace element and isotopic zoning or mantling that reflects the dynamic nature of the open system from which they crystallized.

The observed ranges of isotopic values in the feldspar grains from the Deer Isle Granite Complex, especially

between the alkali feldspar cores and their plagioclase mantles, indicate that there was contamination of the system during formation of these minerals, i.e., there was an open system resulting from magma mixing. The innermost cores of the alkali feldspars share common Ba, La, Ce, and Pb-isotopic characteristics. Outward from the inner core each of the studied grains, a different crystallization history as revealed by its isotopic and trace-element compositions. Figure 17 shows a schematic depiction of the crystal growth (and resorption) histories of each grain in Ba versus $^{207}Pb/^{206}Pb$. The Ba scale simply portrays an increase or decrease in the liquid Ba concentrations as inferred from both plagioclase analyses and Ba X-ray intensity maps for alkali feldspar. The numbers 1–8 in the figure represent inferred sequential liquid compositions. We suggest that these different compositional histories are indicative of open system development and were caused by the relative movement of each grain through a compositionally varied magma, as discussed below.

Formation of feldspars

Alkali feldspar and rapakivi cores

Compositions of the innermost cores of all grains examined, both rapakivi and unmantled alkali feldspars, have similar initial Pb-isotope compositions (inferred liquid composition #1 in Fig. 17a–e). An exception to this observation may be with rapakivi grain FP-5-8R1, which has slightly higher Pb-isotopic ratios in its inner alkali feldspar core ($^{208}Pb/^{206}Pb = 0.855$ and $^{207}Pb/^{206}Pb = 2.087$); however, this is based on only one analysis. Each grain (rapakivi and alkali feldspar phenocrysts) also has relatively low Ba concentrations within their inner alkali feldspar cores (Figs. 3d, 4d, 5d, 6d, 8d). This suggests that they all initially crystallized from Ba-poor magmas that had similar Pb-isotopic compositions.

As growth continued, most of the feldspar grains recorded lower Pb-isotope ratios rimward with minor to little change in Ba concentrations, changing the inferred liquid compositions from #1 to #2 in Fig. 17. This drop is more noticeable in grains FP-5-8R1 and FP-4-7R1 (Fig. 17d, e) with only a limited decrease in grains FP-4-1R1 and FP-4-7R2 (Fig. 17a, b). Mixing of the host with a melt with lower $^{208}Pb/^{206}Pb$ and $^{207}Pb/^{206}Pb$ values and relatively low Ba concentrations could account for this change in FP-5-8R1 and FP-4-7R1. The other grains showing a more limited variation in $^{207}Pb/^{206}Pb$ reflect are lesser input of mixing, probably having crystallized at a greater distance from a zone of mixing between two magmas. A grain more proximal to this inferred mixing zone would acquire an isotopic signature more similar to the injected magma than would a grain more distal to the zone of hybridization.

From this point in their growth, the compositions of most of the grains indicate different crystallization histories. Rapakivi grain FP-5-8R1 (Fig. 17d) experienced an increase in its Pb-isotopic ratios just prior to its inferred resorption and mantling (inferred liquids changing from #2 to #3 and #3 to #4 in Fig. 17d). The concentric zonation of plagioclase inclusions (Fig. 6) supports the idea that the grain may have remained proximal to the zone of mixing. Cyclic periods of rapid growth, brought on by its relative movement in and out of the zone of mixing, caused plagioclase crystals to become trapped along the crystallizing front of the alkali feldspar.

Zoning patterns in grains FP-4-1R1 and FP-4-7R2 suggest that liquid compositions change from #3 to #4 in Fig. 17a and from #2 to #3 in Fig. 17b, respectively, indicating that the crystals became entrained into a batch of Ba-rich magma isotopically similar to the initial host prior to becoming resorbed and then mantled by plagioclase. Within some magma chambers, there is evidence for chemical stratification (e.g., Bateman and Chappell 1979; Hildreth and Wilson 2007). The introduction of these grains into a batch of less fractionated host magma (i.e., still rich in Ba and isotopically similar to the initial magma) could account for the observed crystal growth. Just prior to being resorbed and then mantled, FP-4-1R1 was introduced into a batch of relatively Ba-rich magma with lower Pb-isotopic ratios (#4 to #5 in Fig. 17a).

It is noted that although these grains seem to indicate, they experienced different growth histories prior to being mantled, and there is an inferred resorption event. The degree of resorption could have been different for each grain, and therefore, the record of any common crystallization histories that they may have shared just prior to mantling may have been removed. It is, therefore, not intended to suggest that the crystallization histories of these grains are completely captured in the paths, as shown in Fig. 17.

Rapakivi and plagioclase feldspar mantles

Magmas responsible for plagioclase mantle growth on all the studied grains appear to be just as varied in composition as the magmas from which the outer parts of their cores crystallized. For double mantle of crystal FP-3-1R1, growth of its first mantle was in a Ba-poor and isotopically moderate magma (liquid #2 in Fig. 17c); these values being only slightly lower than ones seen throughout its core (liquid #1 in Fig. 17c). After initial resorption and then mantling of the alkali feldspar core by plagioclase, FP-3-1R1's newly formed plagioclase mantle experienced a major heating event, resulting in the coarse-sieve texture of its inner mantle (Hibbard 1981, 1994; Fig. 5). Its second, or outermost mantle, grew from a Ba rich with similar Pb-isotopic values (# 3 in Fig. 17c) which appears to be similar to the magma

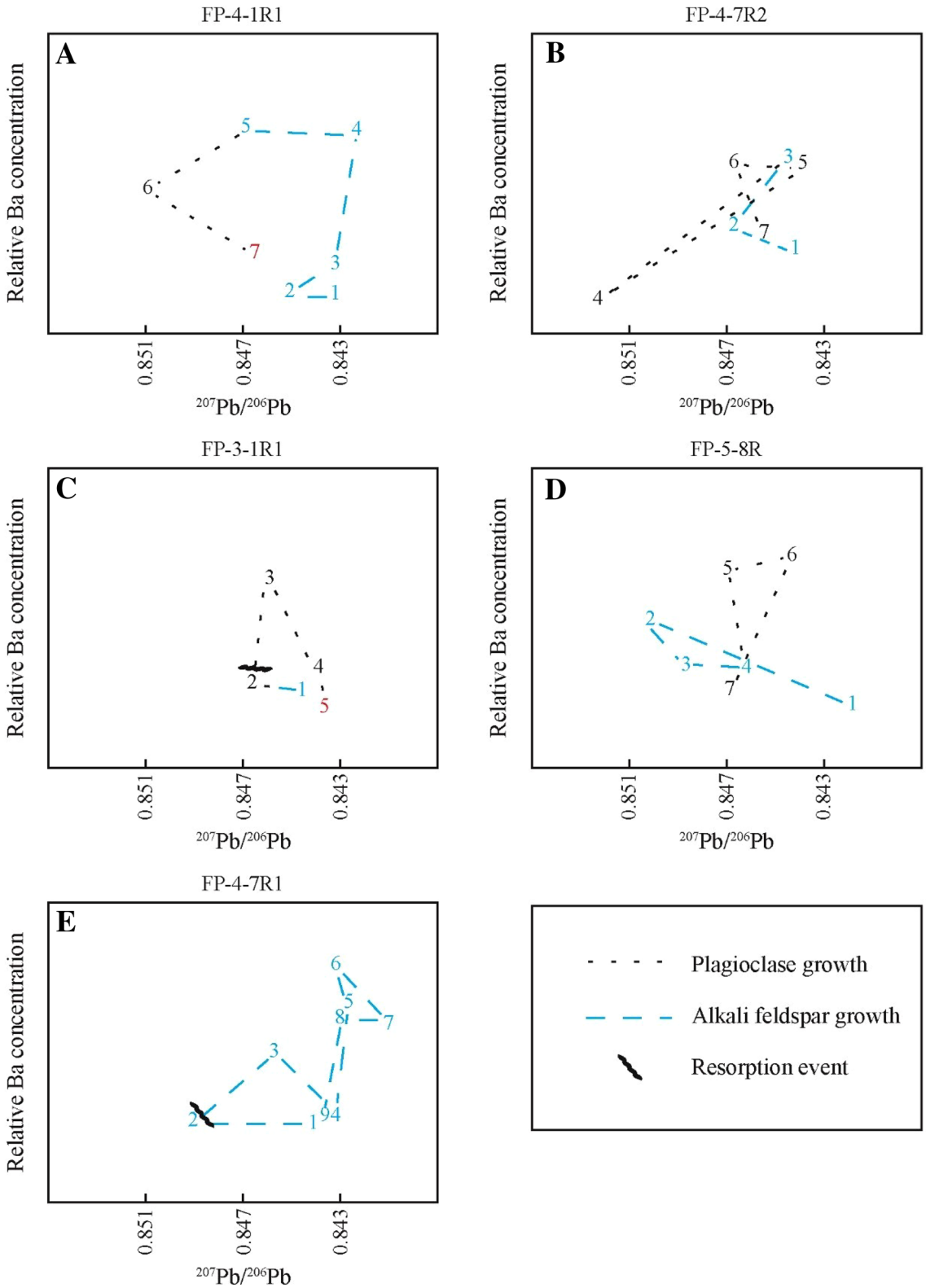

Fig. 17 Schematic crystal growth/resorption histories in relative Ba/^{207}Pb/^{206}Pb space for rapakivi (**a**–**d**) and alkali feldspar (**e**) grains from the Flye Point facies of the Deer Isle Granite Complex. Scale for Relative Ba concentrations is 0–500 ppm for plagioclase and 0–60 counts per second for alkali feldspars (taken from Ba-element maps). Numbers 7 and 5 in **a** and **c** indicates albitic growth

from which FP-4-1R1 and FP-5-8R1 initially crystallized their mantles (liquids #5 in Fig. 17a, d).

The double mantle of FP-4-7R2 displays a different crystallization history than that described above for grain FP-3-1R1. FP-4-7R2, for instance, shows a large drop in Pb-isotopic ratios and Ba concentrations when initial growth of its mantle started (inferred liquid composition from #3 to #4 in Fig. 17b). For FP-4-7R2, no major resorption occurred between its first and second mantling events. Upon further crystallization, a second mantle on rapakivi FP-4-7R2 precipitated from magma that was initially rich in Ba, La, and Ce, with moderate–high Pb-isotopic ratios (#4 to #5 in Fig. 17b). The grain then grew from a liquid with comparable Ba concentrations but with lower Pb-isotopic ratios.

The difference between these two grains could be the result of each grain's relative proximity to a zone of mixing/hybridization could account for this difference in textures. While FP-3-1R1 could have been entrained more thoroughly into the replenishing (hotter) magma, FP-4-7R2 remained more distal. However, then, both mantles appear to have eventually been exposed to a melt that was depleted in Ba and LREEs with no change isotopically. This punctuated decrease in trace-element concentrations is independent of changes in the Pl mantle's An content, which remains ~ An_{20} for both (Figs. 12, 13).

Noticeably different than these rapakivi grains is the isotopic profile of alkali feldspar phenocryst FP-4-7R1. As with other alkali feldspar cores, the growth of its core was within a Ba-poor magma with high Pb-isotopic ratios (liquid #1 in Fig. 17e). As crystallization of the core continued, the magma became progressively lower in its Pb-isotopic values (Figs. 16, 17e, liquids #1 to #2). At this point crystallization stopped and minor resorption of the grain occurred ("r" Fig. 8d). When crystallization again proceeded, its rim (which we interpret to be the equivalent of the plagioclase mantle on the rapakivi feldspars) started growing from a more Ba-rich melt with variable Pb-isotopic values produced by mixing (liquids #2 to #3, then from #3 to #4 in Fig. 17e). Further crystallization of the rim produced homogeneous isotopic values, but fluctuating Ba concentrations (liquids 4–7 in Fig. 17e). This grain must have initially experienced the thermal and compositional perturbation from an injecting magma, but because it was more distal from the zone of mixing than others alkali feldspars that were resorbed and mantled by plagioclase, it never developed into a rapakivi feldspar, because it lacked the strong temperature change present in the mixing zone. This suggests that the injection of magma into the chamber and the proximity of each grain to the chemically diverse and thermally charged magmas were a key to the formation of the diverse types of phenocrysts and rapakivi grains.

The final trend of all the grains appears to indicate that the residual magma had high Pb-isotopic values. The final isotopic signature of the outermost rims is very similar to that of the inner alkali feldspar cores, indicating that the effects of mixing diminished as the grains returned to the dominant, relatively homogenous isotopic composition of the main chamber (e.g., liquids #1 and #7 of Fig. 17b, liquids #1 and #5 of Fig. 17c, etc.). As the grains became separated from the zone of mixing, either in time or space or both, they were adjacent to interstitial melts that evolve to lower Ba, La, and Ce concentrations by fractionation of Ba-rich (alkali feldspar and biotite) and LREE-rich (titanite and allanite) phases, creating the trace-element depletion trends seen in the margins of these grains.

Thus, a plausible scenario immerges from the geochemical and textural evidences that indicate an initial alkali feldspar–plagioclase–quartz-crystallizing magma with $^{208}Pb/^{206}Pb$ and $^{207}Pb/^{206}Pb$ values of ~ 2.08 and 0.85, respectively, and with low Ba and LREE concentrations. The crystals from this magma were actively mixed with a magma with lower $^{208}Pb/^{206}Pb$ and $^{207}Pb/^{206}Pb$ values that were also Ba- and LREE-rich. That magma need not have been mafic in composition; in fact, it may have been granitic in the general sense, but slightly more mafic than the initial Deer Isle magma. According to Ayuso and Bevier (1991), the neighboring Devonian Blue Hill granite has $^{208}Pb/^{206}Pb$ and $^{207}Pb/^{206}Pb$ values of 0.837 and 2.059, respectively. Mixing between the initial Deer Isle magma and a melt that was similar to that which formed the Blue Hill granite could have created the changes in the Pb-isotope ratios seen in the analyzed feldspar grains of the Deer Isle Granite. No published elemental data were found for the Blue Hill granite, and thus, a comparison of major or trace elements could not be made.

Inferences from quartz phenocrysts

Ti concentrations in quartz have been used to indicate changes in temperature during crystallization (Wark and Watson 2006). CL intensity in quartz is typically directly related to Ti concentrations and provides an image of the crystalline results of changing temperatures. Normal zoning (Ti poor, darker rims) indicates the natural decrease of temperature during cooling and crystallization and the opposite trend indicates quartz crystallized from progressively hotter magmas. Thus, as suggested by Müller et al. (2008), Ti–rich mantles on quartz phenocrysts (i.e., more luminescent in cathodoluminescence imaging) might represent the quartz equivalent of a rapakivi feldspar. Thus, quartz phenocrysts should provide evidence of the same events recorded by the rapakivi feldspars. In fact, the reverse zonation of quartz shown in Fig. 9 suggests that temperatures (and/or concentrations of Ti) oscillated, but were higher when the rims crystallized, a pattern similar to that seen in the plagioclase-mantled grains of alkali feldspar.

Truncation of internal growth zones (Fig. 9, white arrows) suggests that the interaction of magmas with different temperatures caused repeated episodes of resorption of the quartz phenocryst. This record of thermal perturbations suggests that this quartz grain crystallized near a mixing zone in the chamber. With each pulse of hotter magma, Ti concentrations within the quartz increased either solely due to the thermal change or possibly also due to an increase in Ti within the magma. Ti enrichment of quartz can be analogous to Ba enrichment in alkali feldspar or plagioclase crystals seen in the Deer Isle Granite, and thus, a similar mechanism is also suggested for the growth of these quartz phenocrysts.

Chamber dynamics

Within the outcrops of the Flye Point facies, neighboring minerals show very different growth zonations (Fig. 2a). Rapakivi feldspars are seen in contact with unmantled alkali feldspar grains and discrete phenocrysts of plagioclase. Like other granitic bodies studied around the world (e.g., Gagnevin et al. 2007), neighboring alkali and rapakivi feldspars (e.g., FP-4-7R1 and FP-4-7R2) have zoning with different Pb isotopes and trace-element concentrations, indicating that they experienced different growth histories. FP-4-7R2, FP-3-1R1, and FP-6-1P1 show two growth events of plagioclase feldspar, yet FP-5-8R1 and FP-4-1R1 do not show this in their mantles, only having one mantle. This juxtaposition of grains with disparate histories, therefore, indicates that they did not grow in situ and must have originated from different parts of the chamber and were subsequently deposited next to each other. As shown in Fig. 2a, complex rapakivi feldspar composite grains are dispersed with simple euhedral alkali feldspars that show no evidence of resorption. Either a decompression model or a simple magma-mixing origin cannot account for the in situ crystallization of disparate crystals, as both the decline in pressure or changes in temperature should have affected all the alkali feldspar (and Qz) crystals. Hence, a different magmatic process must have accumulated crystals with different histories to a common location.

Although cumulates forming in granitic magmas may be problematic from a viscosity perspective, we think that the model by Lux et al. (2007) is the best explanation for the juxtaposition of disparate feldspar crystals (Fig. 18). They describe a vertically zoned magma chamber, with each zone represented by the individual facies of the granite complex (Fig. 1). According to this model, the Flye Point facies represent the bottom-most portion of the chamber, where crystals first started to accumulate. A framework of touching phenocrysts of alkali feldspars, plagioclase, and quartz, with finer grains of the same phases and mafic silicates and

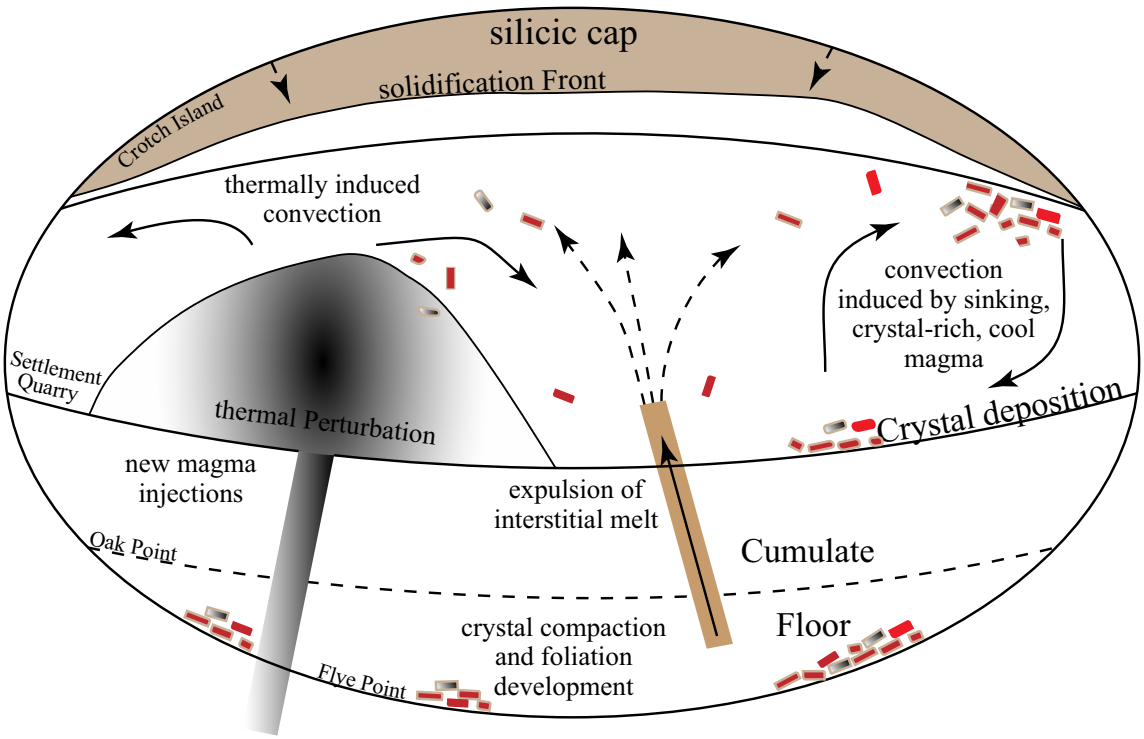

Fig. 18 Theoretical cross section of the Deer Isle Granite Complex (modified from Lux et al. 2007) showing the development of rapakivi feldspars as a result of magma mixing. Refer the text for more description

accessories infilling the interstitial spaces, is consistent with this idea (Chappell and Wyborn 2004; Collins et al. 2006). As cumulates continued to be deposited, the floor of the chamber moved upward with the Oak Point facies representing the last active cumulate surface prior to solidification.

As crystals grew, evidence of their proximity to a zone of hybridization, and the geochemical composition of the magma in which they formed, was texturally and chemically imprinted on each grain. Replenishment of the magma chamber by new magmas caused both the thermal perturbation and locally changed the composition of the magma over time. Crystals could have experienced either mild resorption (e.g., FP-4-7R1), severe resorption (e.g., FP-3-1R1) or possibly no resorption at all depending on how close they were to the center of mixing. Their interaction with varying amounts of this new magma, and to what extent thorough mixing had occurred, resulted in the differences in their isotopic signatures and zoning profiles.

Lux et al. (2007) envisioned that as the magma cooled, a solidification front migrated in from the top and sides of the chamber. Along this front, crystal-rich batches of magma formed and created a density inversion with relatively dense, cooler crystal-rich magma over top less dense hotter crystal-poor magma. These relatively cooler batches of magmas then settled "*en masse*" creating gravity currents. As these currents of crystal-rich magma reached the floor of the chamber, crystals separated out and were deposited. Subsequent depositions of new batches of could potentially carry with them minerals from very different parts of the chamber, allowing for the juxtaposition of two or more minerals with different crystallization histories.

As accumulation increased, compaction caused filter pressing of the cumulate pile, removing interstitial melt (Lux et al. 2007). This silica-rich and less dense interstitial melt rose, through dikes (aplites), into the hotter and more active core of the chamber. This extraction of residual melt led to the leucocratic nature of the Settlement Quarry and Crotch Island facies (Lux et al. 2007). Compaction of the cumulate pile also developed the framework of touching feldspars and feldspar foliation seen within the Flye Point and Oak Point facies (Lux et al. 2007).

The juxtaposition of disparate alkali feldspar phenocrysts in the Deer Isle Granite has bearing on the method of pluton assembly. Glazner et al. (2004) presents the idea of incremental emplacement as a mechanism for the formation of some plutons. In their model, only a small percentage of the pluton contains melt at any one time. Growth of the pluton occurs by amalgamation of small injections of magma (e.g., sheeted dikes) over millions of years. Glazner et al. (2004) further state that the pluton is annealed after emplacement; thus, concealing the contacts of these sheeted dikes. It is evident that for the Deer Isle Granite Complex, there needed to be a large enough chamber, so that several grains could experience completely different histories, be transported away from these sites of magma mixing, and then accumulate together on the floor of the chamber (Fig. 18).

Conclusions

Isothermal decompression (Nekvasil 1991) and magma mixing (Hibbard 1981; Wark and Stimac 1992) have both been proposed to explain the origin of rapakivi feldspars. The Devonian Deer Isle Granite Complex of the Coastal Maine magmatic province was chosen to test these hypotheses. The Deer Isle contains abundant rapakivi feldspars, feldspar phenocrysts, and zoned quartz phenocrysts. Trace-element and Pb-isotopic profiles of the feldspars, coupled with X-ray maps and CL images of quartz and feldspar, indicate that changes in magma composition produced rapakivi feldspars. These changes required an open system (i.e., magma mixing) and are inconsistent with the closed system, isothermal decompression model for the origin of rapakivi textures in this complex. Evidence from rapakivi feldspars, alkali feldspars, and quartz phenocrysts shows that repeated episodes of magma mixing/replenishment (along with more normal fractional crystallization) caused significant temperature and chemical changes during the growth of the crystals. The proximity of grains to mixing zones varied the extent to which each grain was affected by thermal perturbation, thereby permitting the crystallization of rapakivi feldspar with different crystallization histories from the same magma body. While some alkali feldspars only became mantled with Ba-rich feldspar, others experienced one or more plagioclase mantling events (forming rapakivi feldspar). Other alkali feldspar crystals show no resorption or mantling, indicating that these grains were not proximal to the mixing zones. *En masse* settling of crystal-rich mushes brought crystals from different parts of the chamber together and formed the cumulate texture seen within. Juxtaposition of these grains, with different crystallization histories, suggests that a magma chamber of sufficient size must have existed.

Acknowledgements We gratefully acknowledge the assistance of Adam Kent, Richard Bradshaw, and Matt Loewen with the trace element and isotopic analyses at Oregon State University. We are also grateful for the helpful reviews by two anonymous reviewers. This research was supported by the College of Physical and Mathematical Sciences, Brigham Young University.

References

Ayuso RA, Bevier ML (1991) Regional differences in Pb isotopic compositions of feldspars in plutonic rocks of the Northern Appalachian Mountains, U. S. A, and Canada: a geochemical method of terrane correlation. Tectonics 10(1):191–212

Bateman PC, Chappell BW (1979) Crystallization, fractionation, and solidification of the Tuolumne Intrusive Series, Yosemite National Park, California. Geol Soc Am Bull 90:465–482

Boggs S Jr, Krinsley D (2006) Application of cathodoluminescence imaging to the study of sedimentary rocks. Cambridge University Press, Cambridge

Bussy F (1990) The rapakivi texture of feldspars in a plutonic mixing environment: a dissolution-recrystallization process? Geol J 25(3):319–324

Chappell BW, Wyborn D (2004) Cumulate and cumulative granites and associated rocks. Resour Geol 54(3):227–240

Collins WJ, Wiebe RA, Healy B, Richards SW (2006) Replenishment, crystal accumulation and floor aggradation in the megacrystic Kameruka Suite, Australia. J Petrol 47(11):2073–2104

Dailey SR, Christiansen EH, Dorais MJ, Kowallis BJ, Fernandez DP, Johnson DM (2018) Geochemistry of the fluorine-and beryllium-rich Spor Mountain Rhyolite, western Utah. Am Miner 103:1228–1252

Dempster TJ, Jenkin GRT, Rogers G (1994) The origin of rapakivi texture. J Petrol 35(pt. 4):963–981

Eklund O, Shebanov AD (1999) The origin of rapakivi texture by subisothermal decompression. Precambr Res 95:129–146

Gagnevin D, Waight TE, Daly JS, Poli G, Conticelli S (2007) Insights into magmatic evolution and recharge history in Capraia Volcano (Italy) from chemical and isotopic zoning in plagioclase phenocrysts. J Volcanol Geotherm Res 168(1):28–54

Glazner AF, Bartley JM, Coleman WG, Taylor RZ (2004) Are plutons assembled over millions of years by amalgamation from small magma chambers? Geol Soc Am Today 14(4/5):4–11

Haapala I, Rämö OT (1992) Tectonic setting and origin of the Proterozoic rapakivi granites of southeastern Fennoscandia. Trans R Soc Edinb Earth Sci 83:165–171

Heinonen AP, Andersen T, Rämö OT (2010) Re-evaluation of rapakivi petrogenesis: source constraints from the Hf isotope composition of zircon in the rapakivi granites and associated mafic rocks of Southern Finland. J Petrol 51(8):16871709

Hibbard MJ (1981) The magma mixing origin of mantled feldspars. Contrib Mineral Petrol 76(2):158–170

Hibbard MJ (1994) Petrography to petrogenesis. Prentice Hall, Upper Saddle River

Hildreth W, Wilson CJN (2007) Compositional zoning of the Bishop Tuff. J Petrol 48:951–999

Hogan JP, Mataragio JP (2006) Temporal evolution of crustal sources for granitic magmatism in Maine. Geol Soc Am Abstr Programs 38(2):32

Hogan JP, Sinha AK (1989) Compositional variation of plutonism in the Coastal Mine Magmatic Province: mode of origin and tectonic setting: a model. Maine Geol Surv Stud Maine Geol 4:1–33

Hooks BP (2003) Petrology of the Deer Isle Pluton, coastal Maine: a complex mixed magma system [Master's thesis]: University of Maine. Orono, Maine

Johnston B (2001) Magmatic enclaves and evidence for magma mixing in the Oak Point Granite, Deer Isle, Maine, U.S.A. [Master's thesis]: University of Maine, Orono, Maine

Kent AJR (2008) In-situ analysis of Pb isotope ratios using laser ablation MC-ICP-MS: controls on precision and accuracy and comparison between Faraday cup and ion counting systems. J Anal Atomic Spectrom 23(7):968–975

Kent AJR, Jacobsen B, Peate DW, Waight TE, Baker JA (2004) Isotope dilution MC-ICP-MS rare earth element analysis of geochemical reference materials NIST SRM 610, NIST SRM 612, NIST SRM 614, BHVO-2G, BHVO-2, BRC-2G, JB-2, WS-E, W-2, AGV-1 and AGV-2. Geostand Geoanal Res 28(3):417–429

Lux DR, Hooks B, Gibson D, Hogan JP (2007) Magma interactions in the Deer Isle Granite complex, Maine: field and textural evidence. Can Mineral 45:131–146

Mondal A, Upadhyay D, Banerjee A (2017) The origin of rapakivi feldspar by a fluid-induced coupled dissolution-reprecipitation process. J Petrol 58:1393–1418

Müller A, Breiter K, Seltmann R, Pécskay Z (2005) Quartz and feldspar zoning in the eastern Erzgebirge volcano-plutonic complex (Germany, Czech Republic): evidence of multiple magma mixing. Lithos 80(1–4):201–227

Müller A, Seltmann R, Kober B, Eklund O, Jeffries T, Kronz A (2008) Compositional zoning of rapakivi feldspars and coexisting quartz phenocrysts. Can Mineral 46:1417–1442

Narayana BL, Mallikharjuna Rao J, Subba Rao MV, Murthy NN, Divakara Rao V (2000) Geochemistry and origin of Early Proterozoic Dongargarh rapakivi granite complex, Central India—an example for magma mixing and differentiation. Gondwana Res 3(4):507–520

Nekvasil H (1991) Ascent of felsic magmas and formation of rapakivi. Am Miner 76:1279–1290

Rämö OT, Haapala I (1995) One hundred years of rapakivi granite. Mineral Petrol 52:129–185

Rämö OT, Haapala I (2005) Rapakivi granites. In: Lehtinen M, Murmi PA, Rämö OT (eds) Precambrian geology of Finland—key to the evolution of the fennoscandian shield. Elsevier B. V, Amsterdam, pp 533–562

Sederholm JJ (1891) Ueber die finnländischen Rapakiwigesteine. Tschermaks Mineralogisch-Petrographische Mitteilungen 12:1–31

Stewart DB (1956) Rapakivi Granite of the Deer Isle Region, Maine [Ph.D. thesis]: Harvard University, Cambridge, Massachusetts

Stimac JA, Wark DA (1992) Plagioclase mantles on sanidine in silicic lavas, Clear Lake, California: implications for the origin of Rapakivi texture. Geol Soc Am Bull 104:728–744

Stull RJ (1979) Mantled feldspars and synneusis. Am Miner 64(5):514–518

Vernon R (2016) Rapakivi granite problems: plagioclase mantles and ovoid megacrysts. Aust J Earth Sci 63(6):675–700

Vorma A (1976) On the petrochemistry of rapakivi granites with special reference to the Laitila massif, southwestern Finland. Geol Surv Finland Bull 285:1–98

Wang X, Wang T, Haapala I, Mao J (2008) P-T conditions of crystallization and origin of plagioclase-mantled K-feldspar megacrysts in the Mesozoic granitoids in the Qinling orogeny (China). Lithos 103(3):289–308

Wark DA, Stimac JA (1992) Origin of mantled (rapakivi) feldspars: experimental evidence of a dissolution- and diffusion-controlled mechanism. Contrib Mineral Petrol 111(3):345–361

Wark DA, Watson EB (2006) TitaniQ: a titanium-in-quartz geothermometer. Contrib Mineral Petrol 152(6):743–754

Whitney JA (1975) The effects of pressure, temperature and X_{H2O} on phase assemblage in four synthetic rock compositions. J Geol 83(1):1–31